University of Twente

EEMCS / Electrical Engineering
Control Engineering

Automobile tire profile measurement

Armen Karapetian

MSc Report

Supervisors:
prof.dr.ir. P.P.L. Regtien
prof.dr.ir. W.C. van Etten
Jan van Londen, Van Londen Bandenservice

October 2007

Report nr. 026CE2007
Control Engineering
EE-Math-CS
University of Twente
P.O.Box 217
7500 AE Enschede
The Netherlands

Summary

The goal of the project is to develop an automatic tire profile measurement system. Nowadays various commercially available sensors could be used for such distance measurements.

During the project different sensors and methods for distance measurements are studied. The measurement performance depends on several factors such as physical structure of the measured object, the measurement environment and the methods to acquire information. The project is started with an analysis of the measured object where the physical structure, the form of the object, and the changes in these factors during the tire life time are considered.

Three major non-destructive sensor groups are discussed in the report: optical, acoustic and imagers. According to the requirements and performance/cost factors the most suitable examples from each group of sensors is analysed and evaluated by experiments. As a result an active sensing method based on a coded light active triangulation system, consisting of a camera and a pattern projector, is chosen for the realization of a demonstrator.

Finally the demonstrator is realized and extensively tested and is operational at the Laboratory for Measurements and Instrumentation.

Samenvatting

Het doel van dit onderzoek is de ontwikkeling van een automatische systeem voor het meten van bandprofieldieptes. De huidige commercieel beschikbare sensoren zouden het mogelijk moeten maken dit soort afstanden nauwkeurig te kunnen meten.

Gedurende het onderzoek zijn verschillende sensoren en diverse methodes voor het meten van de profieldieptes onderzocht. De functionaliteit van een meetsysteem is afhankelijk van enkele factoren: de fysische structuur van het meetobject, de meetomgeving en de methoden waarop de informatie wordt verkregen. Het project is begonnen met een analyse van de structuur en de vorm van het meetobject. Ook de veranderingen in deze factoren gedurende de gebruiksduur van het meetobject zijn in beschouwing genomen.

In het rapport zijn drie groepen van niet-destructieve meetmethoden behandeld: optische, akoestische en imaging sensoren. Gegeven de systeemeisen ten aanzien van functionaliteit en kosten is van elke groep de meest geschikte methode geanalyseerd en experimenteel geëvalueerd. Dit heeft geresulteerd in de keuze voor een meetmethode gebaseerd op triangulatie met gecodeerd licht. Er is een demonstrator gerealiseerd bestaande uit een camera en een optische patroongenerator. Uit uitgebreide testen met deze demonstrator is gebleken dat de gekozen methode een goed uitgangspunt vormt voor verdere ontwikkeling van het meetsysteem.

Preface

This report describes my Doctoral assignment of Electrical Engineering study at the University of Twente.

I would like to thank Paul Regtien for providing me with this interesting assignment and being always helpful when I had problems.

I would also thank Alfred de Vries for being always ready to answer my questions and for the maintenance of a good-humoured work sphere in the Lab.

Armen Karapetian

Enschede, October 2007.

Here's an old trick:

If one uses a penny and can see the top of Lincoln's head, it is time to recycle that tire.

Contents

1 Introduction

The car tire condition is highly important for economical and environmental reasons. Tire pressure and the profile depth are essential parameters and that is why these are the most frequently inspected tire characteristics. Nowadays tire inspection takes place in a service centre with involvement of a specialist. The measurements of a profile are done manually using a ruler. This results in a labor-intensive inspection process with demurrage of a car process.

A system is needed to support the measurements of the tire pressure and the profile and to communicate with a service centre. Several different options have been investigated to design a system for the measurements and for communication purposes. The overall result will be a demonstrator of a wireless profile monitoring system.

The design of a subsystem for profile measurement system is a subject of this report.

1.1 Requirements

The information received from the tire profile measurement system will be used for different purposes such as computing the worn out date of the tire. Therefore a correct and precise measurement of the tire profile is needed. The required precision of the measurement system is 0.1 mm. The measured distance range is from 1.5 to 20 mm. These are the minimal and the maximal (new) profile depths. To recover a tire profile contour the measurements of a profile groove of 2 mm width is required.

The measurement system should fit in the wheel fender. Because of the system's placement a construction of a protection against water, dirt and stones will be needed. This should be taken into account during the design of the measurement system. The protection should be realizable. The profile depth of each tire of the vehicle will be measured.

The measurements will be done at a standstill of the car.

1.2 Assignment

This research is a joint project with a Dutch company that sells and services tires for different automobiles. One of the services is changing the tires when their profile is worn out. For an accurate planning of this procedure a precise tire measurement is required. The precision of the measurement must be better than 0.1 mm.

During the project a feasibility study on different non-destructive measurement methods will be carried out. Traditional distance measurements are based on optic, acoustic and visual (with camera and image processing) methods. These will be verified for usage in this particular case.

The final setup will consist of a demonstrator (a measurements setup), integrated in a wireless monitoring system.

1.3 Report outline

Chapter 2 discusses the background information of the measured object: a truck tire. The measurement environment and the three basic nondestructive measurement methods are also considered in Chapter 2. Chapters 3, 4, 5 describe the study and the experimental results of each of the optical, acoustic and imager based measurement systems. The results are summarized and compared in conclusions in the Chapter 5. Also recommendations for future work are proposed in this chapter.

2 Background

The physical structure and the geometrical form of the object in combination with the measurement environment are the basic factors for the choice of the measurement method. This chapter gives the background information of the tires. Also the environmental aspects are discussed in this chapter. Further, general information on non-contact distance measurement sensors is given in this chapter.

2.1 Analysis of the measured object and environment

The goal of the project is to develop a method for measurements of tire profile depth. To develop a universal measurement method for different types of tires knowledge about the structure and the geometrical shape of the tires is needed.

2.1.1 Physical structure

The architecture of the tire is illustrated in Figure 1.

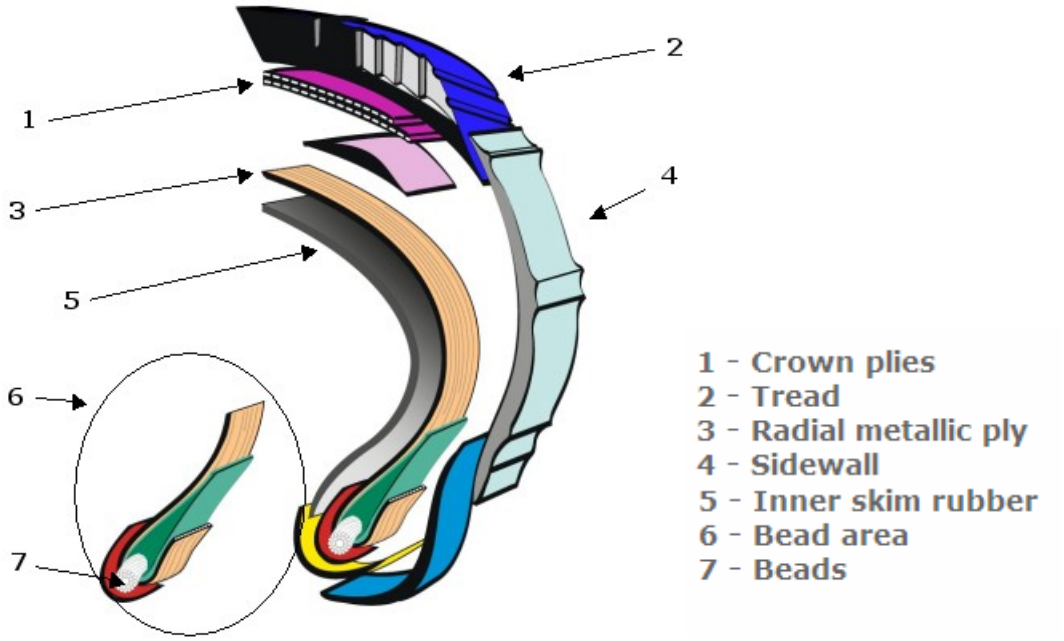

Figure 1: Tire architecture

The radial tire with next characteristics is used as an example:
- a flexible casing with the bracing plies laid at right angles to the casing ply
- a metallic bracing is used to stabilize tread movement
- the tread and sidewalls operate independently.

Metal and rubber are the basic elements used in the tire construction. But there is a trend to replace the metallic elements with plastic. That is why measurement methods based on metal detector sensors must be excluded. The tire color is black. So, the measurement systems based on color detection will be impossible. The black color of the measurement object could result in difficulties when methods based on light reflection will be applied.

2.1.2 Geometrical form of the tire profile

Generally all tires can be divided in three categories according to there position on the truck:

- Steer tire
- Traction tire
- Trailer tire

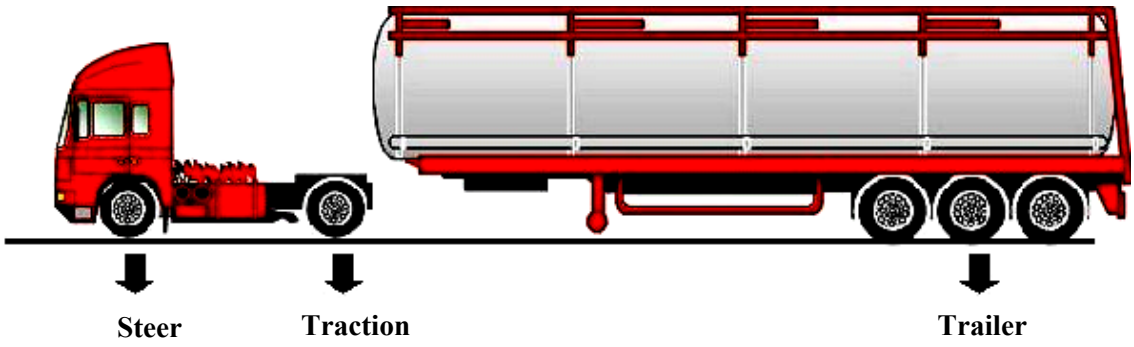

Figure 2: Tire differences per position on a truck

For different weather and road conditions special type of tires should be used. As example, the tire marking of Michelin according to the exploitation environments is illustrated in Figure 3.

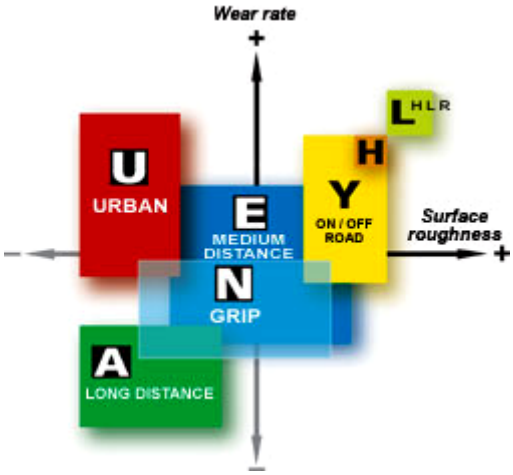

Figure 3: Tire code

The fact that there are more than ten major tire manufactures which produce steer, traction and truck tires for different weather and road conditions results in a huge range of different tire profiles. To design a universal measurement system for all different tires two major different approaches are possible:

- Design of an object independent measurement system
- Locate a general classification factor (physical or geometrical aspect) for all tires, and design a universal algorithm based on this classification factor.

The first approach is preferable.

For the measurement methods where the geometry of the object is crucial the classification of tires according to their specific geometry (classification factor) will help to develop a measurement method.

The main issue of finding the specific geometry is that this geometry must be identifiable throughout the tire's life. For example if one groove is chosen as a classification factor it must be visible till the tire is worked out.

Most of the steer and trailer tires have a longitudinal groove as illustrated in Figure 4 (a, b).

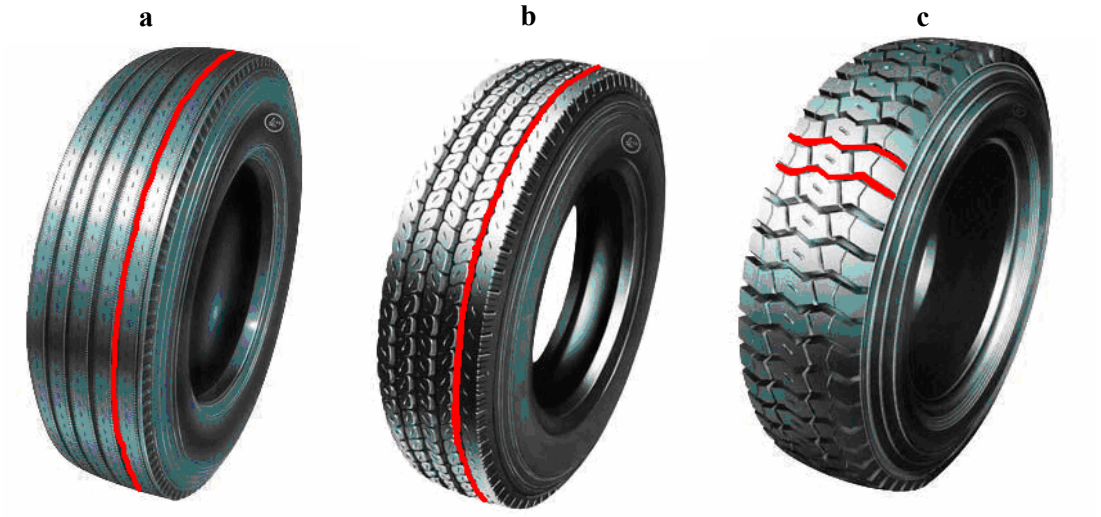

Figure 4: Longitudinal (a, b) and inclined (c) grooves

Only the steer and trailer tires developed for off road conditions does not have longitudinal grooves. The groove can have different forms: from a straight line (Figure 4 a) to sinusoidal (Figure 4 b) or others. The presence of the longitudinal groove in traction tires is similar to steer and trailer.

The position of the inclined grooves (see Figure 4 c) on a particular tire depends on usage in a vehicle, exploitation environment and on tire manufacturing. Because of unpredictability of the position and the form this groove can not be used as a universal classification factor of the tires.

2.1.3 Measurement environment

The performance (sensitivity, reliability, etc.) of the measurements depends on the sensing method and the environmental conditions. For example mechanical sensors are independent on the lightning of the object but could fail for temperature ranges below 0 degrees. Conversely an imager (camera) could not be used in a dark environment but will have the same performance for temperature ranges from -30 to 50 ^{o} C. Knowledge about the measurement environment is needed for a proper sensor choice. Next to environmental conditions, essential for the choice of the measurement methods are: lightning, mechanical conditions, electro-magnetic conditions, acoustical conditions and temperature.

Lightning

The measurement system will be mounted in the wheel fender. In general the lightning of the tires is poor. As the measurement system will be used on different trucks and at different positions on the truck the lightning of the tire will change per truck and per position. When an imager is used for sensing purposes an extra lightning source is needed. For measurement systems where the environmental light could interfere the performance the conditions in the wheel fender are defined as favorable.

Mechanical conditions

Because the measurements will be performed at a standstill of the truck there are no vibrations during measurements. But the measurement system should be resistant to vibrations during the truck exploitation.

Electro-magnetic conditions

The electro-magnetic condition of the measurement environment could be described as a hash free. There are no instruments or details in the wheel fender which could be expected in the generation of the electro-magnetic field.

Acoustical conditions

These conditions are important if acoustic sensors are used for profile measurements. The quality of an acoustic measurement strongly depends on the acoustic properties of the environment and the measured object. The environment is the air and the measured object the tire, both with known acoustic properties. Because the measurements will be done in the wheel fender possible wave reflections should be taken into account.

Temperature

The measurement system will be used world wide and in every season of the year. This results in a temperature range from -40 to 40 ^{o} C where the measurement system should perform reliable.

2.2 Non-contact measurement systems

A wide range of sensors are available for the non-contact distance measurements. Generally all commercially available sensors for non-contact distance measurements could be divided in three groups:

- Optical (distance detectors)
- Acoustic (based on acoustic transducers)
- Imagers (camera based systems).

This classification is done on the physics of the sensor. Because of the wide range of sensors a variety of methods to acquire information could be applied.

The kind of sensors needed and the method to acquire and process information depends largely on the particular task for which the measurement system will be used for. The required specifications (following from the measurement system task) with respect to range, precision, reliability, price plays the major role in the choice of the sensor.

2.2.1 Optical sensors

Generally, a sensor system operating on optical principles consists of a light source, a light sensor and the transmitting medium (Regtien, 2004). The optical sensor translates the distance changes in changes of transmission, reflection, absorption, scattering or diffraction of a light beam. Also time-of-flight (TOF), phase shift and interference are used in more complex sensor systems.

Next to light sources also emitters are used in a sensor system: thermal light bulb, light-emitting diode (LED), semiconductor laser diode and gas laser. Commonly used sensors are: photo resistor, photo diode, photo transistor, diode array, position sensitive diode (PSD), area scan (CCD/CMOS camera). The main characteristics of the emitters are their radiation spectrum, controllability, moderately focused beam, intensity control. The sensors are characterized according to the sensitivity to light, direction sensitivity, response time, sensitive to color and size.

2.2.2 Acoustic

Similar to optical sensing systems, acoustic sensing systems, too, consist basically of three parts: a source, a receiver and a modulating medium (Regtien, 2004).

Commonly used acoustic sensors belong to one of the types: piezoelectric, electrostatic, electromagnetic and magnetostrictive. Only the first two are suitable for ultrasonic application. The major characteristic of the acoustic sensors is the operating frequency band.

Because of simple construction (see Figure 5) and low cost of acoustic transducers the interest in using this kind of sensors for distance measurements is growing.

Figure 5: Piezoelectric sensor

Most acoustic sensing systems are based on the measurement of the TOF. The traveled distance x follows directly from TOF t, using the relation $v_a = x/t$. The sound signal can be of any shape. The most popular are: burst (number of periods of sine wave), continuous wave with constant frequency (CW) and chirp (continuous, frequency modulated wave). The drawbacks of the methods are different. The burst based methods have a limited precision. The reasons are: the starting point of the echo pulse can not be detected accurately and the noise or reflections mask the arrival time of the echo.

For the CW methods it is impossible to use the same transducer to send and receive. The high resolution is only achievable at a fixed distance, because the distance is obtained from the phase difference of transmitted and received waves.

Combining burst and CW techniques results in a method with advantages of both techniques. The distance is calculated as follows:

$x = \frac{\Delta f \cdot v_a}{2 \cdot k \cdot f_0}$, where Δf is the frequency difference between the transmitter and receiver, k the linear coefficient of frequency variation and f_0 the amplitude of the wave.
The major disadvantage of this method is that only wide band transducers can be applied. Also a complex interfacing is required.

2.2.3 Imagers

Most imagers use a camera and a proper illumination scene. The image (or a sequence for 3D reconstruction) is analyzed by some image processing algorithm applied to the intensity distribution in the image. From particular patterns in the light intensity in the image particular object features are extracted. Combining the information on camera parameters (position, orientation and focal length) and position of the features in the image the real-world position information could be derived.

Specified conditions for getting a proper image must be fulfilled: an illumination that yields adequate contrast and no disturbing shadows; a camera set-up with a full view on the object or the scene and with a camera that has a sufficiently high resolution, not to lose relevant details (Regtien, 2004).

During the identification and reconstruction from an image different difficulties could arrive: occlusion (hidden behind other object or the object's part), acquisition of the object perspective aspect. Even in the most favorable situation, the image alone does not reveal enough information for a specific task.

The needed information is:

- Object model
- Imaging process model.

Using this information the pose of the object in the scene can be derived from the available information and knowledge of the imaging system.

Different strategies for obtaining 3D shape information from 2D images have been studied: stereovision, methods based on "structured light". But the sufficiency of the methods depends on the particular task requirements.

2.3 Conclusions

Combining information about the measured object, environment and different measurement possibilities some conclusions could be done.

Measurement methods based on metal detectors are not suitable for this project.

For the classification of the tire according to their form a longitudinal groove can be used as a classification factor. All tires can be divided in two general groups:

- With a longitudinal groove (Figure 4 (a,b))
- Without a longitudinal groove (Figure 4 c)

According to the group pertinence of the tires different measurement algorithms can be applied. In the later stadium two different algorithms can be integrated in one measurement method. This is one of the approaches which gives a possibility to develop a universal method for all tire types.

Imperfections of the sensors are usually listed in the datasheets provided by manufacturer. Unfortunately, many datasheets show lack of clarity and completeness. One of the reasons is the varying sensor performance for different tasks and environment.

To choose the best suitable sensor type for tire profile measurements the following is done:

- From each group of the sensors: optical, acoustic, imagers, the most appropriate sensor with the best performance/price factor is selected. For defining the performance the next sensor parameters will be compared: sensitivity, robustness, implementation complexity (mechanical construction and signal post processing).
- A comparative study on the selected sensors is performed. Results will be compared resulting in which sensor is most favorable for the tire profile measurements.

Because a camera will be used for visual control of the tire profile, it is also preferable to develop a measurement method where the same camera could be utilized in the measurements setup. According to this fact all sensors are divided in two groups: one with and another without use of an imager (camera).

3 Non-imagers

This chapter describes the measurement systems based on optical and acoustic sensors. Each section begins with a theoretical background of each kind of sensors. Then a description of the test setup and the results of verification experiments are given.

3.1 Optical sensors for tire profile measurements

In the past few years, several new infra-red detectors have been introduced by producers. With the introduction of the new generation of sensors, a new approach is used that not only gives object detection at a longer range than the previous methods, it also offers range information. These detectors offer a small package (see Figure 6), very little current consumption, and a variety of output options.

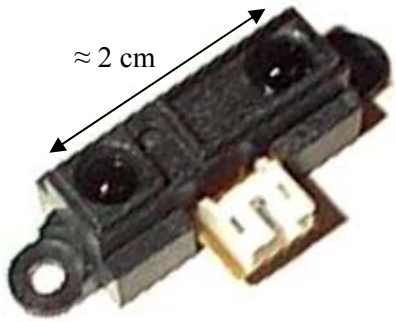

Figure 6: Example of an optical sensor Sharp GP2D120J00F

The sensors offer much better immunity to ambient lighting conditions because of the new method of ranging.

These sensors all use triangulation and a small linear CCD array to compute the distance and/or presence of objects in the field of view. The basic idea is this: a pulse of IR light is emitted by the emitter. This light propagates in the field of view and either hits an object or just keeps on going. In the case of no object, the light is never reflected and the reading shows no object. If the light reflects off an object, it returns to the detector and creates a triangle between the point of reflection, the emitter, and the detector.

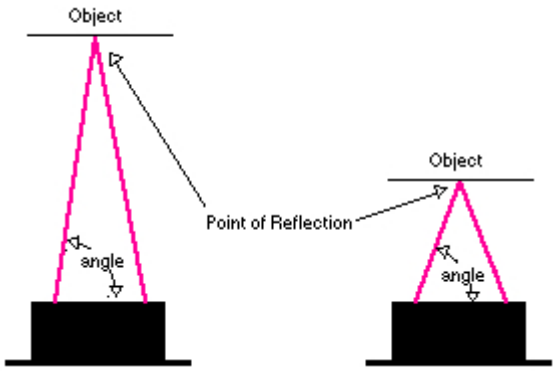

Figure 7: Different Angles with Different Distances

The angles in this triangle vary according to the distance to the object. The receiver part of these new detectors is actually a precision lens that transmits the reflected light onto various elements of the enclosed linear CCD array based on the angle of the triangle described above. The CCD array can then determine what angle the reflected light came back and, therefore, it can calculate the distance to the object.

This method of measuring is almost immune to interference from ambient light and offers amazing indifference to the color of the object being detected. Measurements on a black wall in full sunlight are possible.

There is a series of GP2XXX detectors which vary in several respects. The Sharp GP2D120J00F was chosen for test purposes as being most suitable for the profile measurements. From the GP2XXX series this sensor is developed to work over the shortest distance ranges, smaller than 40 cm, what is encouraging for the project. This also results in a highest achievable sensor resolution for the GP2XXX series.

According to sensor producer the output of the detectors (analog voltage) is non-linear with respect to the distance being measured because of some basic trigonometry within the triangle from the emitter to reflection spot to receiver. In Figure 8 the characteristic of the Sharp GP2D120J00F is illustrated.

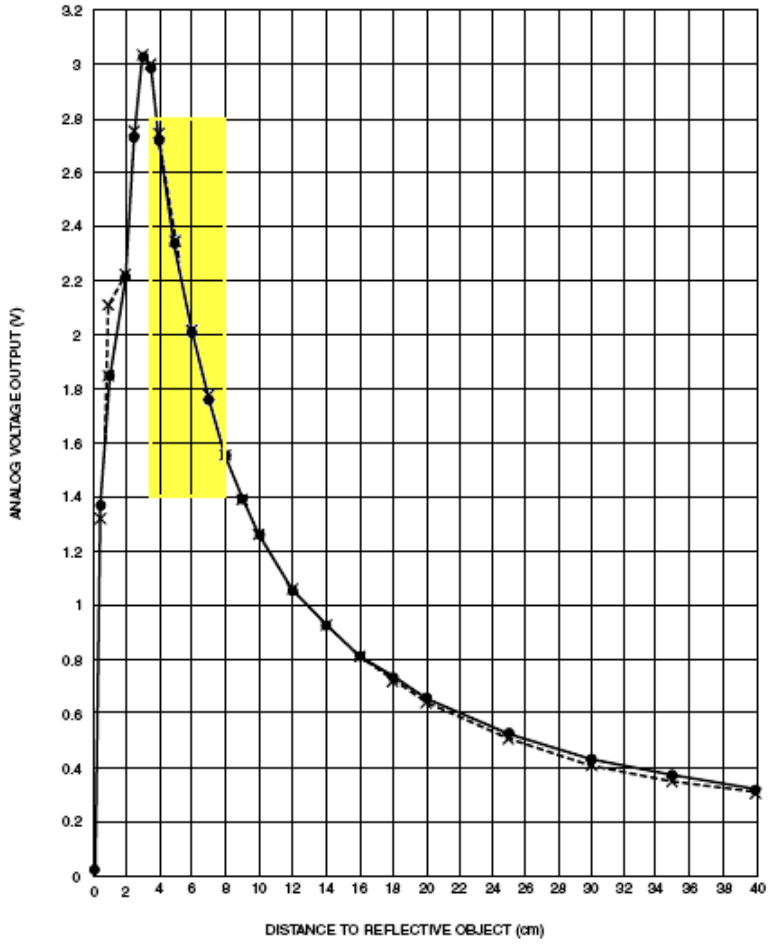

Figure 8: Output voltage to distance

Following the sensor characteristic from Figure 8 the best measurement resolution could be achieved for the measurements of the objects at distances of 3.5 to 8 cm from the sensor. At that interval (marked area) the characteristic has the most abrupt form and it is nearly linear. For the measurements in this area a constant coefficient could be used to convert the output voltage of the sensor to distance. This coefficient is calculated as followed:

$$C = \frac{80-37}{2.8-1.6}\left[\frac{mm}{V}\right] \approx 36\left[\frac{mm}{V}\right].$$

The performance of the sensor will be tested in this range. Furthermore, the non-linear voltage output of the sensor could be converted to a usable distance measure. One way to do this is to find a function that converts the output voltage into a range value. According to the datasheets of the sensor for the distances to reflective objects below 3 cm the measurements of the sensor are not reliable.

3.1.1 Measurement setup

The recognition of shapes requires a set of distance sensors or scanning with a single sensor. In the test setup a method based on scanning is applied. For the object scanning a movement across the object is

needed. For this purpose an X-Y recorder is used. The sensor is mounted on the moving part of the recorder what gives a possibility to scan the objects in one of the X or Y direction. The distance from the sensor to the closest area of the object is ≈40 mm. The precise distance between object and sensor is not of interest because only relative measurements are carried out. The linear displacement of the sensor in the movement direction could be achieved from the recorder.

Two different tests are done to control the sensor performance. The first one is conducted to verify the sensor's general performance and the second one to test the precision of the sensor. For the first part a dark object with slots of various depth (h) and width (w) is used.

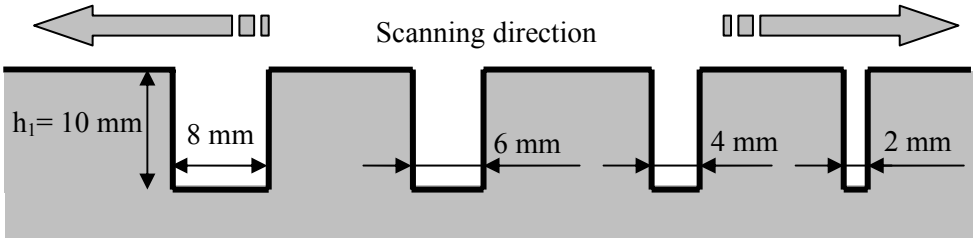

Figure 9: First test object

In Figure 9 the illustration of a dark colored object with slots with depth h_1 = 10 mm and a various width is given. Three objects with the same form but different depth (d_1 = 10 mm, d_2 = 5 mm, d_3 = 2 mm) are available for the test purpose. These objects simulate the truck tires with different profile form. The measurements on all objects should provide a reliable result. Otherwise the sensor could not be used for the profile measurements.

To test the precision of the sensor an object as illustrated in Figure 10 is used.

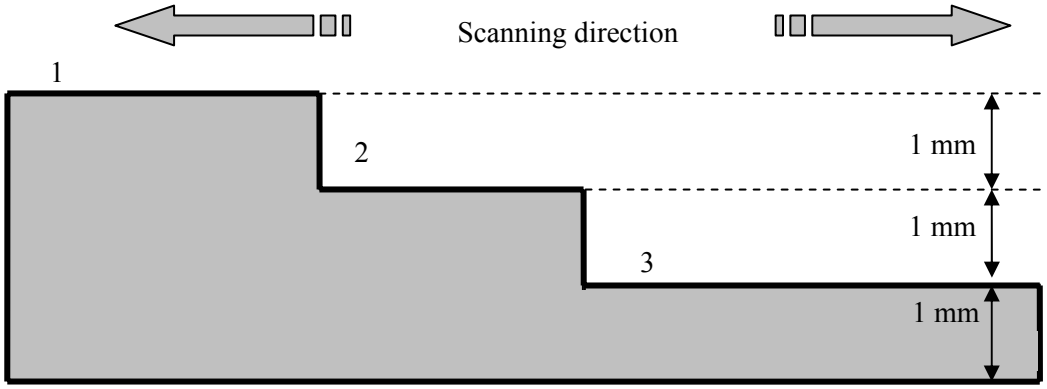

Figure 10: Second test object

The required precision of the measurements is tested and the maximal precision of a particular sensor could be achieved from the tests. The results of both tests will be used to verify the information derived from the producer.

3.1.2 Test results

Before testing the precision of the Sharp sensor some calculations based on the characteristic illustrated in Figure 8 and the required precision could be performed. As was mentioned the sensor is positioned at $D_1 \approx 40$ mm from the object. Suppose the maximal depth of the measurement object is D_2 = 20 mm. Using this information the change in voltage output when the distance is changed with 0.1 mm can be calculated as follows:

$$\frac{\Delta D}{\Delta V} = \frac{60-40}{2.8-2}\left[\frac{mm}{V}\right] = \frac{0.1}{4}\left[\frac{mm}{mV}\right] \qquad (1)$$

From this calculation it is clear that when the distance changes with 0.1 mm this should result in a change in the sensor output voltage of 4 mV.

3.1.3 General performance test

The test is started using the object with largest depth and width. If the performance of the sensor meets the requirement the test is continued with the objects of smaller size.

Figure 11 illustrates the result (Figure 11 a) and the object (Figure 11 b) of the measurements with depth $\Delta d_1 = 10$ mm and width $w_1 = 8$ mm.

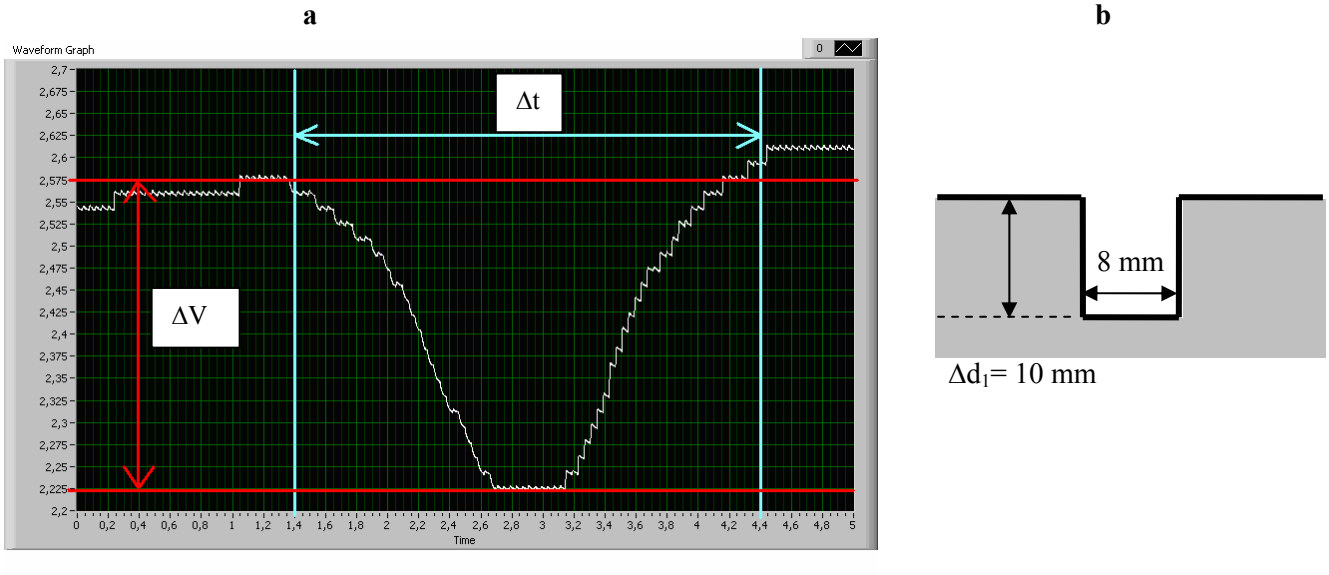

Figure 11: Measurement result (a) and the measured object (b) with the optical sensor

From observations of the test results it is concluded:

- The detection of the object's depth is possible. But there are fluctuations in the measurements corresponding to the same distance
- The detection of the precise position of the object's contour directly from the sensor output is impossible. Signal post processing and/or usage of object's model is required
- The output voltage of the sensor is changing in steps what can result in low precision. This will be studied during the precision test.

The following calculation is carried out according to the information of the sensor output from Figure 11.

The horizontal axis of the characteristic is the time of the measurements and the vertical- voltage output of the sensor. Using Figure 8 the voltage output could be converted to the distance:

$$\left.\begin{array}{l} V_1 = 2.575[V] \rightarrow d_1 = 45[mm] \\ V_2 = 2.225[V] \rightarrow d_2 = 55[mm] \end{array}\right\} \Delta d = 10[mm]$$

Because of fluctuations in the output voltage the average value V_1 of 4 local maxima is used in the calculation of the object depth.

Also the time of the measurements can be converted to the distance (object's width), according to the scanning speed: $1[\text{sec}] = 4[mm]$. Because the exact contour of the profile is not detectable the values of the time as shown in Figure 11 are used for calculation. This will give an indication of the sensor performance when the object's contour measurements are needed.

$$\Delta t = 4.4 - 1.4[\text{sec}] = 3[\text{sec}] \rightarrow w = 12[mm]$$

The real width of the object is 8 mm. Obviously, the sensor data for width detection show a too low accuracy for reliable measurements. This becomes more visible when the object's width decreases. In Figure 12 the measurement of the object with a depth of 10 mm and width of 2 mm illustrated.

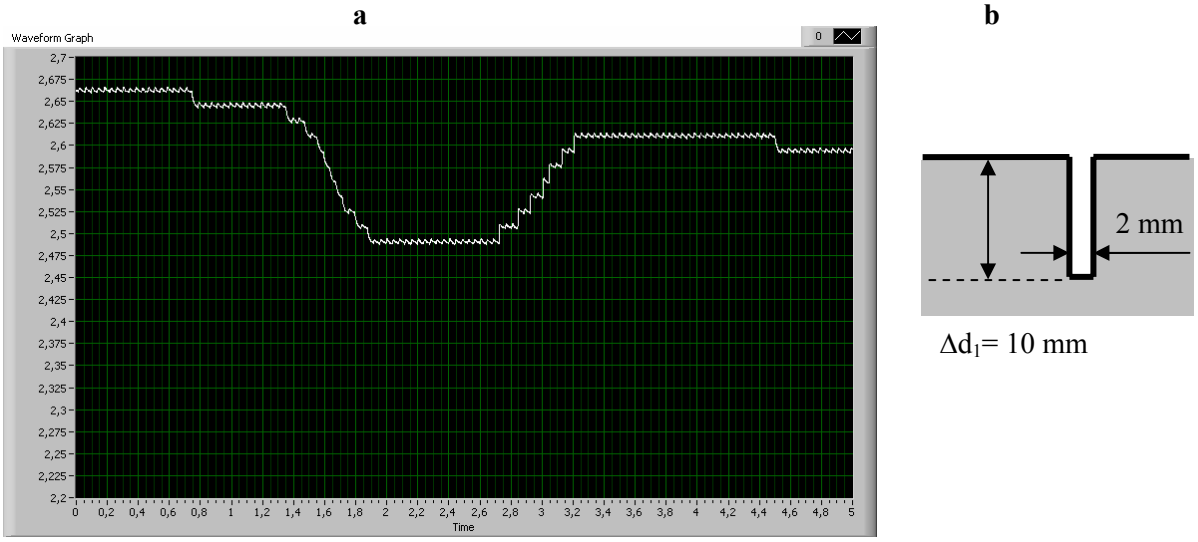

Figure 12: Measurement result (a) and the measured object (b) with the optical sensor

An evident performance degradation of the sensor is visible. The depth of the object measured to be 8 mm and the width when using the method of calculation as in previous test is 5.4 mm. The result does not match the object real size.
The same tests are done under different lighting conditions of the environment. One of the advantages is that the changes in the sensor performance are not detected.
Summarizing the tests results next conclusions can be made:

- Accurate detection of the objects contour is impossible
- Unstable. Fluctuation of the output also during the detection of the flat surface.

Following test will determine the cause of these fluctuations.

3.1.4 Precision test

The precision of the sensor should be obtained after the test is completed. In Figure 13 test results and the measured object are illustrated.

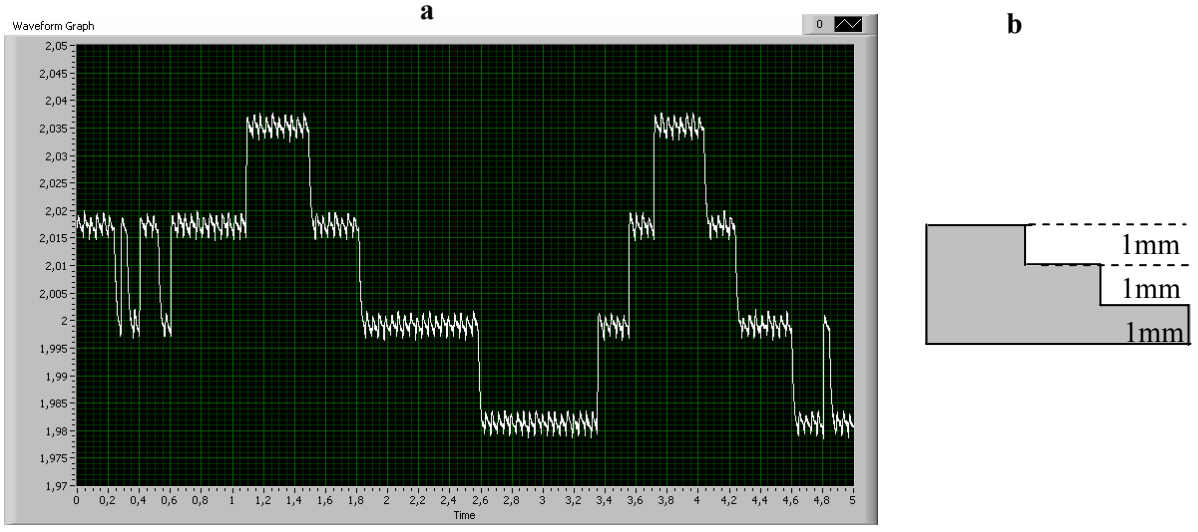

Figure 13: Measurement result (a) and the measured object (b) with the optical sensor

From the precision test next things are visible:

- Sensor fails in detection of the object. In place of expected three steps four steps are visible. Also the measured distance value is not stable.
- The changes in the output voltage have a clear stepwise character. The value of the step is the resolution of the sensor. Converted into distance measurements resolution (*D.M.R.*) this is:

$$D.M.R. = (2.0350 - 2.0155) \cdot 36 = 0.7[mm]$$

The same instability is observed during the scanning of a flat surface. Low sensor resolution results in fluctuation of $\pm 0.7[mm]$ in the measurements value of the flat surface.

- The presence of noise with RMS of 5 mV is observed. In equation (1) the maximal step size of the sensor's output voltage is calculated to be 4 mV to achieve the required precision of distance measurements. A filtering technique should be applied to achieve the needed precision.

The reasons of the stepwise changes of voltage output value is due to intrinsic low resolution of the sensor.

3.1.5 Conclusions

Summarizing the test results the following advantages and disadvantages of the Sharp sensor could be mentioned:

Advantages:

- Simple construction
- Independent from lightning changes
- Low cost

Disadvantages:

- A range of sensors or a scanner mechanism is needed to cover the measurements area
- The non-linear output which could result in a complex computation and calibration procedures
- Low signal-to-noise ratio (without post processing), limiting the sensor precision to 0.7 mm.

3.2 Acoustic sensors for tire profile measurements

Recently, with the remarkable advance of electronics and semiconductor technology highly sophisticated piezoelectric components have come to existence. A piezoelectric ceramic with unique function which can translate electrical to mechanical energy and mechanical to electrical energy was introduced for applications in ultrasonic transducers. With the introduction of efficient, stable and economical devices based on lead titanate, lead zirconate the usage of ultrasonic sensors has broadened.

A series of the Murata's piezoelectric ultrasonic sensors is studied to decide which sensor meets the project requirements.

A MA400A1 sensor with the highest operating frequency (400 kHz) is chosen for the tests because the precision of the measurements directly depends on this frequency. The wave length at 400 kHz in air is nearly 0.8 mm. The detectable range of the sensor according the producer is from 0.06 to 0.3 m with a resolution of 1 mm. One of the other important characteristics of the sensor is its narrow beam (see Figure 14).

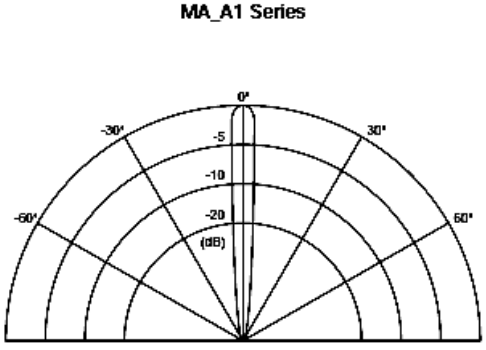

Figure 14: Directivity in overall sensitivity

According to the producer the signal beam of the MA400A1 is 7 degrees. This narrow beam gives the possibility for measurements of small details of the objects.

3.2.1 Measurements setup

For this method two acoustic sensors were used. The setup is illustrated in Figure 15.

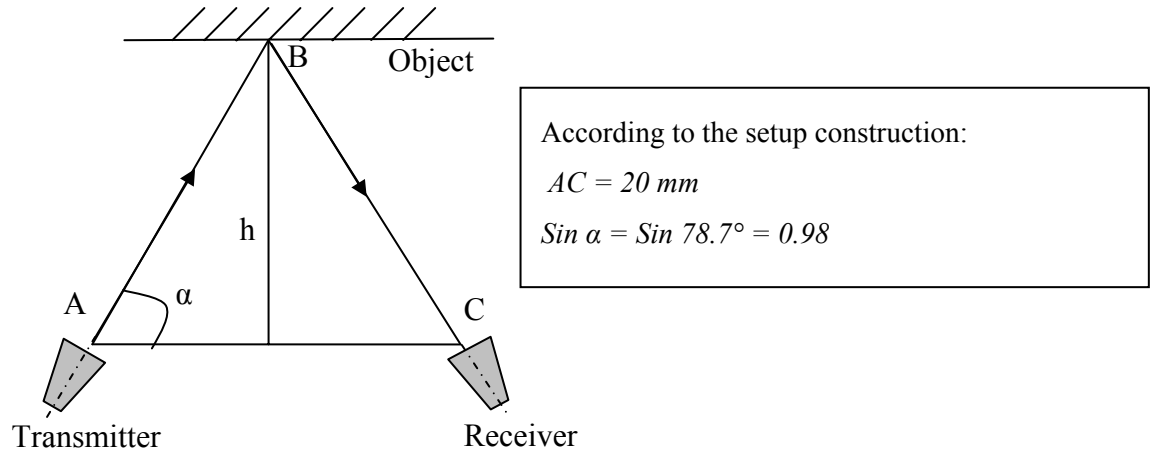

Figure 15: Measurements setup

The distance h must be measured. This measurement system is based on the time-of-flight (TOF) method. The transmitter emits a short burst (circa 10 periods of sine wave) in the direction of an object. The sound reflects, travels back and is received by the receiver. The elapsed time between the excitation of the sound pulse from the transmitter and its arrival at the receiver is measured. The speed of sound in air is about 340 m/s. Using the relation: $x = V \cdot t$, where $x = AB + BC = 2 \cdot AB$, h can be calculated:

$$h = AB \cdot \sin\alpha = 0.5 \cdot V \cdot t \cdot \sin\alpha = 166.7 \cdot t[m] \quad (2)$$

The datasheet of the sensor reports a directivity angle of 7°. When the distance AB from sensor to object is 30 mm the diameter d_s of the signal beam on the surface of the object is:

$$d_s = 2 \cdot AB \cdot \tan(3.5^\circ) = 3.7[mm]$$

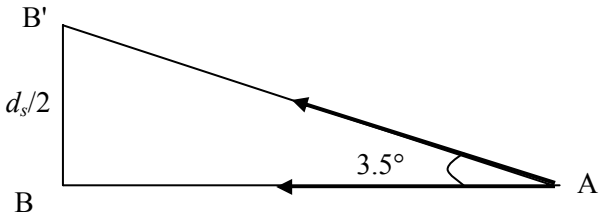

Figure 16: Calculation of the bundle on the object surface

This means that the depth measurement of a 3.7 mm narrow groove will be possible. The verification of this will be done by a general test.

For precision verification the object from Figure 10 will be used.

3.2.2 General performance test

For this test the object illustrated in Figure 9 is used. The measurement system is positioned at 30 mm from the object's nearest surface (see Figure 17 right).

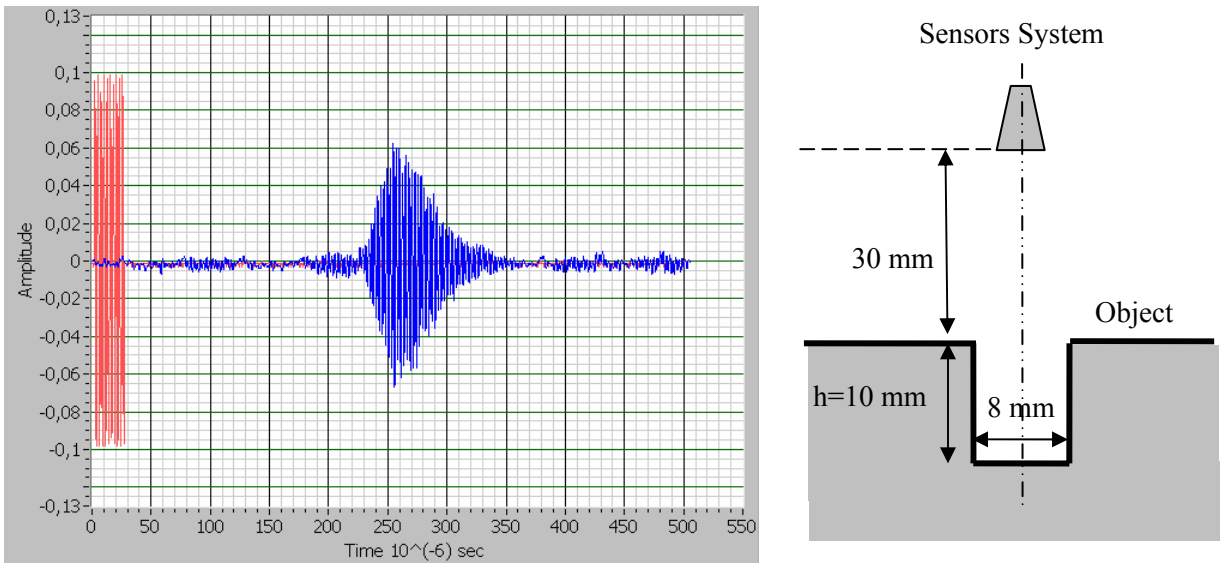

Figure 17: Measurement result (left) and the measured object (right)

A burst signal of 10 periods sine wave with a frequency of 400 kHz is transmitted. Four stationary measurements are done with grooves of 10 mm high and 8, 6, 4 and 2 mm wide. Figure 17 (left) illustrates the experiment result with the object of 8 mm. The echo signal first increases achieving a maximum value and then decreases. The reason for this typical response is the resonance structure of the sensor. Because the beam width is smaller then the groove only one echo signal is visible. This signal is from the bottom of the groove. The situation will change when the groove becomes narrower. Two echo's: one from the bottom and another from the top of the groove, will be received. The experimental results with the grooves of 4 and 2 mm width are illustrated in Figure 18 left and right, respectively.

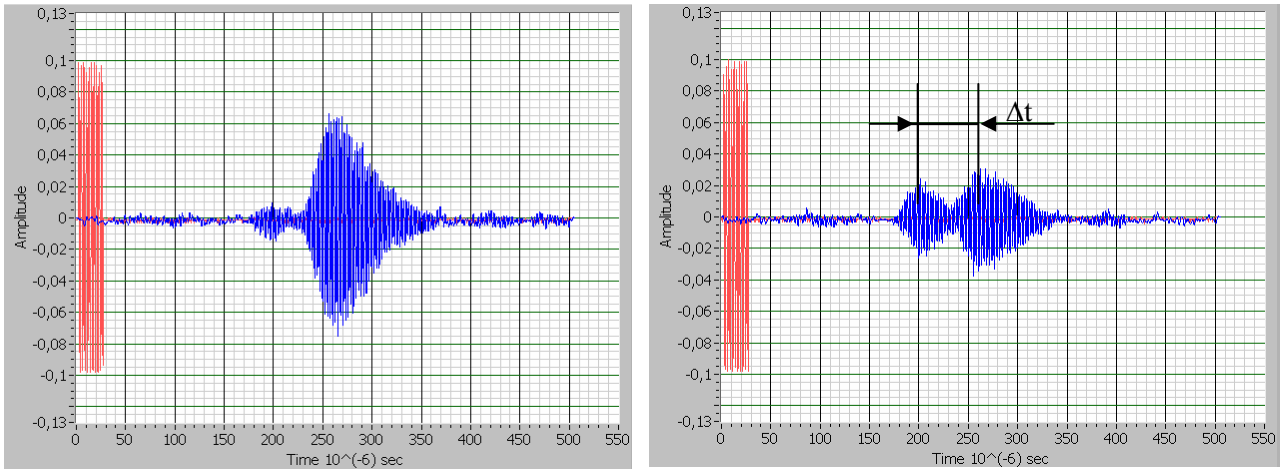

Figure 18: Measurement results on 4 mm (left) and 2 mm (right) wide grooves

The results with grooves of 8, 6 (not illustrated) and 4 mm are nearly the same. The major echo signal comes from the bottom of the groove. This corresponds with the calculation result of the signal beam diameter. When the groove width is nearly two times smaller than the signal bundle two echo's become visible (see Figure 18 right). The presence of two echo signals with nearly the same maximum during the detection of 2 mm groove demonstrates the impossibility of object's contour recognition using the method described above. However, the distance measurement based on measuring the difference between the time arrivals of the maximum in the two echo signals (Δt in Figure 18 right) can lead to reliable results. The disadvantage of the sensor for contour detection could be used as an advantage for distance measurements. This will be discussed in the next section.

Summarizing:

- The detection of the object's depth is possible.

- The detection of the precise position of the objects contour directly from the sensor output is impossible. Signal post processing and/or usage of objects model is required
- Scanning of the profile will result in an increase of system complexity
- Relative distance measurements where the echo signals of the same wave from different surfaces are used could result in a reliable and precise method.

3.2.3 Precision test

The second test object as illustrated in Figure 10 is used for these experiments. This object is placed at a distance of 30 mm from the measurement system. Three experiments are done. The measurement system is statically placed and the object is moved. Both relative and absolute distance calculations are done. For this purpose during the measurements the arrival time of the echo's signal maximum is detected and indicated (*Max Time*) in the following figures.

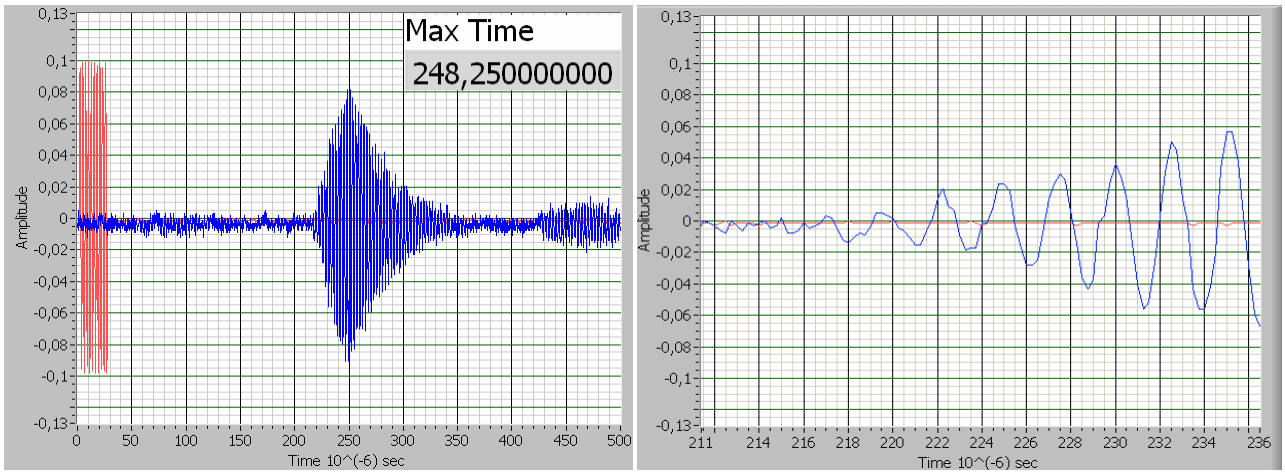

Figure 19: First measurement on a 1mm high object

In Figure 19 the first measurement results are presented. In the right part of this figure a zoomed echo signal is shown. For absolute measurements the starting point of the echo signal is needed. The precision of the measurements depends on the detection of this point. One lost or erroneously detected period of the echo signal corresponds with a distance measurement error of 0.4 mm (half of the wave length).

If we take t = 215 µsec as the starting point of the echo the distance calculated according to the TOF method is: $h \approx 36$ mm. The real distance is 30 mm. When detecting the begin point of the echo from both the left and the zoomed right illustrations in Figure 19 this leads to an unreliable result.

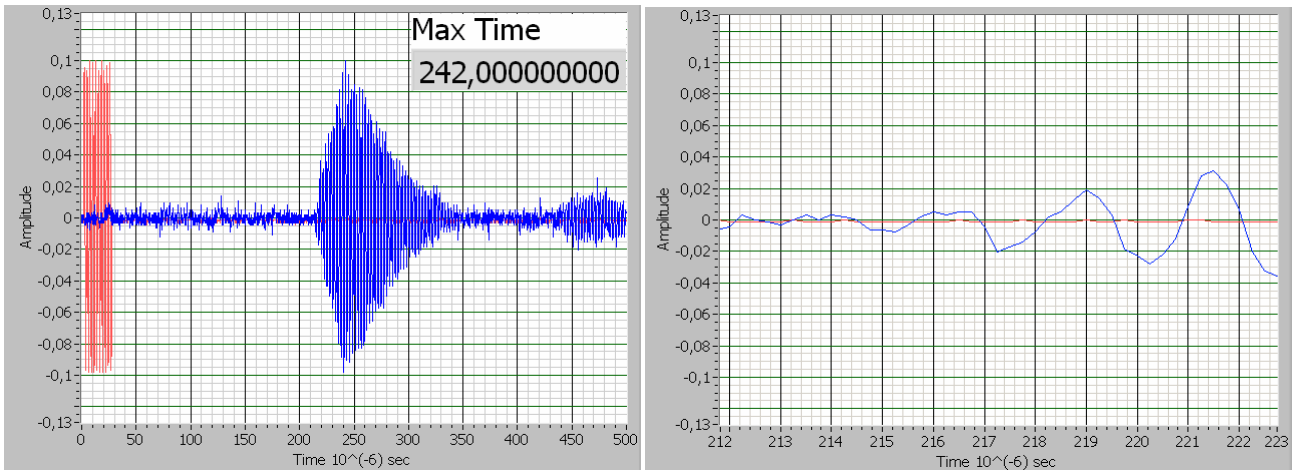

Figure 20: Second measurement on a 1mm high object

Figure 20 illustrates the experimental results when the object is shifted horizontally. This should result in a decrease of 1 mm in the distance between the measurement system and the object. The same

problem of the begin point of the echo detection occurs. But now the relative distance measurement can be applied. According to the measurements:
$\Delta t_{\max} = t_{(1)\max} - t_{(2)\max} = 248.25 - 242 = 6.25\,[\mu\text{sec}] \Rightarrow \Delta h \approx 1[mm]$.

This particular measurement gives a precise result. But the measurement is not reliable because this precision is not always achievable. The precision of the measurements depends on the detection of the maximum of the echo. Anyway this method is more resistant against noise than the detection of the begin point of the echo signal only.

Summarizing the experiment results:

- Absolute distance measurements based on TOF could not achieve the required precision and reliability. The best measurement resolution is 0.4 mm. The measurement's reliability and resolution could increase when the transfer function of the sensor is known. This will give the possibility to use the maximum of the echo signal to calculate the starting point of the echo.
- The relative measurements based on the detection of echo signals maximum are more reliable. Combined with the sensor model (transducers transfer function) this could result in a high precision.

3.2.4 Conclusions

Summarizing the test results the following advantages and disadvantages of the Murata's MA400A1 sensor can be mentioned:

Advantages:

- Simple construction
- Independent from lightning conditions
- Low cost

Disadvantages:

- A range of sensors or a scanner mechanism is needed to cover the measurements area
- The resonant behaviour of the sensor which could result in a complex computation and calibration procedure
- Without post processing and usage of a model: a low sensor precision of about 0.4 mm

3.3 Conclusions

Both tested sensors have a lower precision than required (0.1 mm). For measurements of the whole tire profile a scanning mechanism should be constructed. The scanning procedure of the tire profile could result in a time consuming process.

The possibility to increase optical sensor performance is more unlikely that of the acoustic one. The precision of this sensor is limited by the CCD sensor size, its resolution and the characteristics of the laser light. These can not be changed. The precision of the measurements with the acoustic sensor depends on the operating frequency and the features of the transmitted wave.

4 Imagers

In the last years the generation of 3D models of physical objects has become a topic of research interest. Particular attention has also been paid to depth reconstruction, which can be employed in a wide range of applications such as inspection, navigation, object recognition.

Nowadays the depth reconstruction is mainly achieved using non-contact systems based on light waves, in particular using active or passive sensors (see Figure 21). Active sensors directly provide range data containing the 3D coordinates necessary for the measurement of object depth. Passive sensors provide images that need further processing to derive the 3D object coordinates.

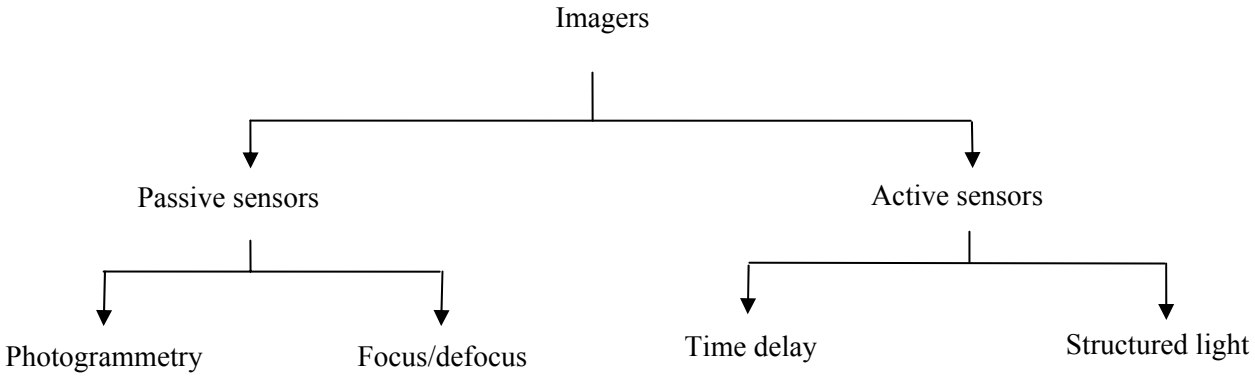

Figure 21: 3D measurements methods

Structured light

Projection of a single spot, sheet of light or a bundle of rays

Time delay

Methods are based on time of flight. The light waves could be modulated or optical interferometry is used.

Focus/defocus

The depth from focus and defocus is used.

Photogrammetry

2D coordinates are used for image measurements (correspondences) to recover 3D object information though a mathematical model. Stereovision is one of the widely used set of methods to obtain 3D information of the object. Image content methods are also part of photogrammetry. These methods detect depth from shading, texture and edges of the object.

The most suitable sensing methods from each group of active and passive sensors for this project will be analytically chosen and evaluated with experiments.

Since the goal of the project is to develop a method for performing metric measurements from images and these images have been acquired using a camera, quantitative models of these devices are needed.

4.1 Camera model

According to the sensing techniques a geometrical or/and physical model of the cameras is required.

4.1.1 A Physical model

The physical model relates the amount of light that is reflected and emitted at a point on an object to the brightness of the image of that point in the retinal plane.

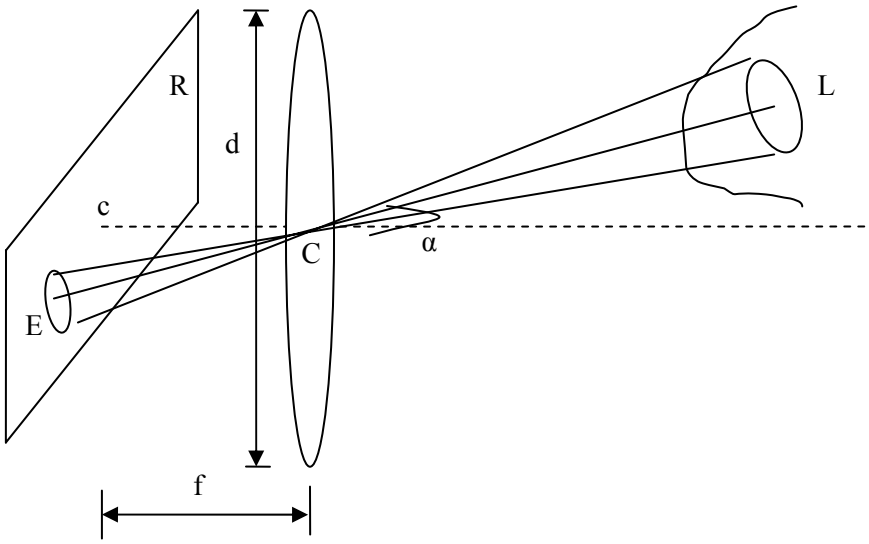

Figure 22: Camera model

The relationship between the image irradiance *E* and the scene radiance *L* can be used for computations:

$$E = L\frac{\pi}{4}(\frac{d}{f})^2 \cos^4 \alpha$$

The parameters involved in this equation are defined in Figure 22, where R is the retinal plane and C is the optical center.

4.1.2 A geometrical model

In measuring the position and orientation of the objects a relationship between camera and world coordinates is required. This section describes the mathematical models of this relationship.

1. **Pin-hole camera model**

A pinhole camera model can accurately model the geometry and optics of most of the modern CCD cameras. Such a camera model consists of a nontransparent plane with a small hole (see Figure 23).

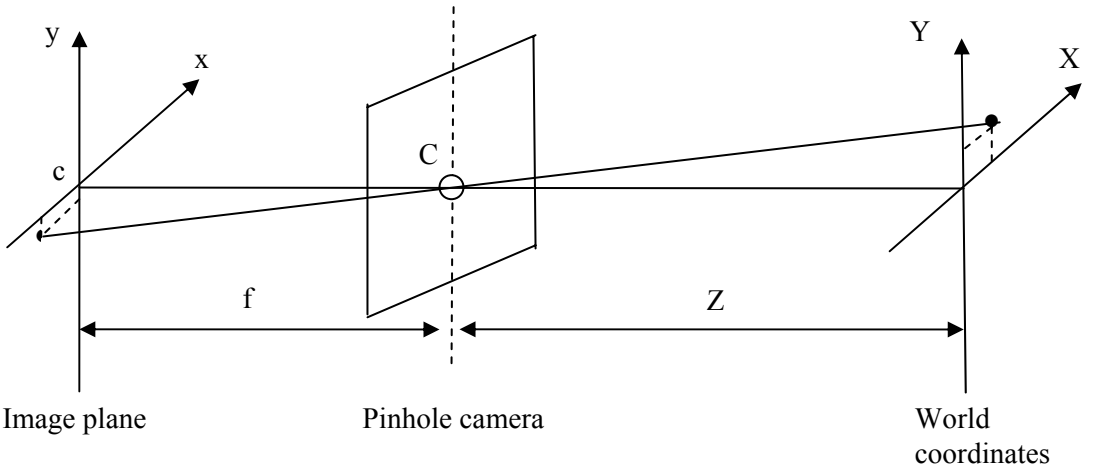

Figure 23: Pinhole camera model

Light emitted from the surfaces of objects in the scene passes though the hole and illuminates the image plane, also called retinal plane. The pinhole camera plane and the image plane are in parallel. The distance between these planes is f, the focal length of the optical system.

In Figure 23 the world coordinates are coupled to the camera without rotation or translation. In other words, the camera and world coordinate coincide. The z-coordinate of the image plane is constant. The relationship between world coordinates and image coordinates is:

$$x = -\frac{X \cdot f}{Z};\ y = -\frac{Y \cdot f}{Z}$$

Each point in the image plane corresponds exactly to one surface patch in the scene. However, from a particular image point one cannot reconstruct the original world coordinate of the patch. One can only deduce the ratio between position (*X* and *Y*) and the depth Z of the emitting path (v.d. Heijden, 1994).

As the goal of the project is recovering 3D information from a single view the so called "ill-posed" problem (for each point there are two equations and three unknown coordinates) applies. The system consisting of one camera is underdetermined. For manmade objects (e.g. tires), geometric constraints on the object (e.g. perpendicularity and orthogonality) can be used to solve this ill-posed problem. But in the case of free objects these assumptions are not valid and another measurements system is needed.

.

2. World Coordinates

Camera parameters are commonly divided into extrinsic and intrinsic parameters. Extrinsic parameters are needed to transform the object coordinates to a camera centered frame. In multi-camera systems the extrinsic parameters also describe the relation between the cameras. The object and the camera coordinates are typically given in a right-handed Cartesian coordinate system. This is illustrated in Figure 24, where the camera projection is approximated with a pinhole model (Heikkilä, 1997). The pinhole model is based on the principle of the collinearity, where each point in the object space is projected by a straight line thought the projection centre into the image plane.

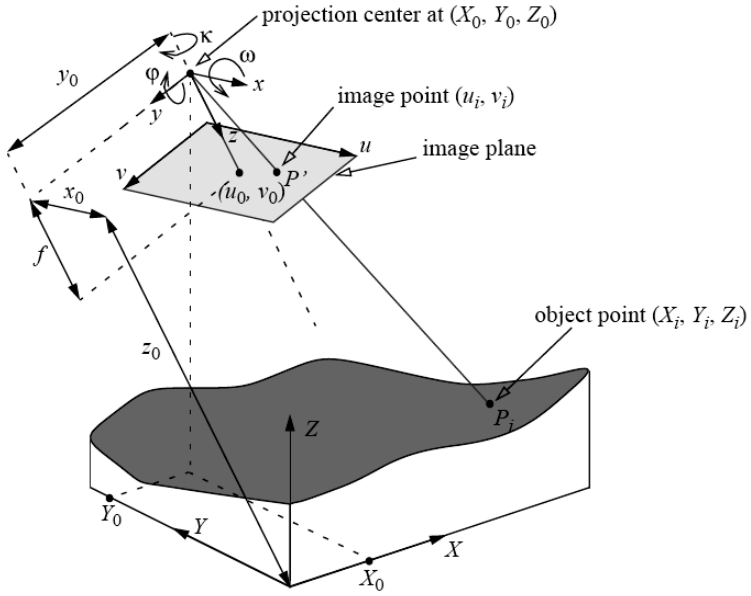

Figure 24: Camera and world coordinates

In order to express any object point P_i at location (X_i, Y_i, Z_i) in the image plane coordinates, a transformation to camera coordinates (x_i, y_i, z_i) is needed. This transformation consists of translation and rotation, which is described with following matrix equation:

$$\begin{bmatrix} x_i \\ y_i \\ z_i \end{bmatrix} = M \cdot \begin{bmatrix} X_i \\ Y_i \\ Z_i \end{bmatrix} + \begin{bmatrix} x_0 \\ y_0 \\ z_0 \end{bmatrix} = \begin{bmatrix} m_{11} & m_{12} & m_{13} \\ m_{21} & m_{22} & m_{23} \\ m_{31} & m_{32} & m_{33} \end{bmatrix} \cdot \begin{bmatrix} X_i \\ Y_i \\ Z_i \end{bmatrix} + \begin{bmatrix} x_0 \\ y_0 \\ z_0 \end{bmatrix}, \quad (3)$$

where

$$m_{12} = \sin\omega \cdot \sin\varphi \cdot \cos k - \cos\omega \cdot \sin k \qquad m_{11} = \cos\varphi \cdot \cos k$$

$$m_{22} = \sin\omega \cdot \sin\varphi \cdot \sin k + \cos\omega \cdot \cos k \qquad m_{21} = \cos\varphi \cdot \sin k$$

$$m_{13} = \cos\omega \cdot \sin\varphi \cdot \cos k + \sin\omega \cdot \sin k \qquad m_{31} = -\sin\varphi$$

$$m_{23} = \cos\omega \cdot \sin\varphi \cdot \sin k - \sin\omega \cdot \cos k \qquad m_{32} = \sin\omega \cdot \cos\varphi$$

$$m_{33} = \cos\omega \cdot \cos\varphi$$

The intrinsic camera parameters include the focal length f, scale factor s_u, which adjusts the image aspect ratio, and the image centre (u_0, v_0). As usually in computer vision, the origin of the image coordinate system is in the upper left corner of the image array. The unit of the image coordinates is in pixels, and therefore conversion factors D_u and D_v are needed to change metric units to pixels. In fact, the precise values of D_u and D_v are not needed, because they are linearly dependent on the focal length f and the scale factor s_u. By using the pinhole model, the projection of the point (x_i, y_i, z_i) to the image plane is expressed as:

$\begin{bmatrix} \tilde{u}_i \\ \tilde{v}_i \end{bmatrix} = \frac{f}{z_i} \begin{bmatrix} x_i \\ y_i \end{bmatrix}$, the values in this equation are metric.

The corresponding image coordinates (u_i', v_i') in pixels are obtained from the projection $(\tilde{u}_i, \tilde{v}_i)$ by applying the following transformation:

$$\begin{bmatrix} u_i' \\ v_i' \end{bmatrix} = \begin{bmatrix} D_u s_u \tilde{u}_i \\ D_v \tilde{v}_i \end{bmatrix} + \begin{bmatrix} u_0 \\ v_0 \end{bmatrix}$$

The pinhole model is an approximation of the real camera operation. It is a useful model that enables simple mathematical formulation for the relation between object and image coordinates. However, it is not valid when high accuracy (<1 pixel) is required, and therefore, a more comprehensive camera model must be used. Usually, the pinhole model is a basis that is extended, with some corrections, for systematic distortions.

A commonly used camera model is derived by combining the pinhole model with the correction for radial and tangential distortion components (Heikkilä, 1997):

$$\begin{bmatrix} u_i \\ v_i \end{bmatrix} = \begin{bmatrix} D_u s_u (\tilde{u}_i + \delta u_i^{(r)} + \delta u_i^{(t)}) \\ D_v (\tilde{v}_i + \delta v_i^{(r)} + \delta v_i^{(t)}) \end{bmatrix} + \begin{bmatrix} u_0 \\ v_0 \end{bmatrix} \qquad (4)$$

The effects of radial and tangential distortion are illustrated in Figure 25.

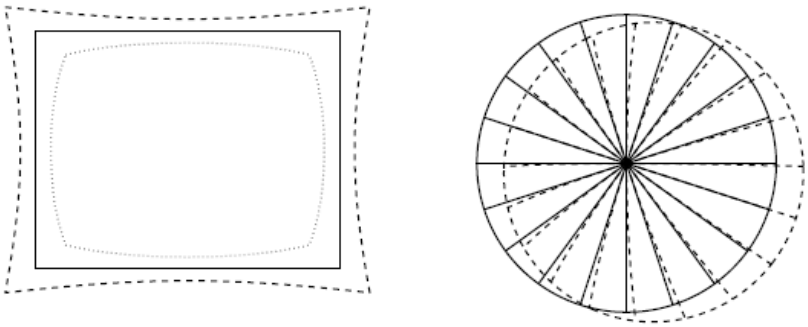

Figure 25: Radial and tangential distortion

Some other distortion types have also been proposed in the literature. For example, linear distortion, thin prism distortion. In most cases, the error is small and the distortion component is insignificant.

4.2 Passive sensors

Passive sensors provide images that need further processing to derive the 3D object coordinates. The complexity of the reconstruction algorithms depend on many factors: sensing method, knowledge about measured object, models used to describe the imaging and the object (Remondino and El-Hakim, 2006).

This section discusses the advantages and disadvantages of different passive sensing methods. Different photogrammetry methods such as Stereovision and Image content are highlighted. The focus/defocus method is described in this section. The most suitable for tire profile measurements are verified with experiments. Conclusions of degree of applicability of passive close this section.

Image content

Compared with the other passive sensors this measurement method uses the most simple measurement setup, which basically consists of one camera. From the image made with the camera the object will be reconstructed.

In some cases, the shape of an object can be estimated from only a single image by analyzing the image content like edges and contours, how the light/shading varies across the surface of the object, and how the texture of the object is distorted by the orientation and the shape of the surface of the object.

For measurements on the tire profile the longitudinal groove could be used to find the edges for further post processing and depth recovering. But because of the tire position a special lightning will be needed.

A general draw back of this measurement method is the computational problem of the ill-posed camera, as explained in 4.1. This means that the 3D information should be reconstructed using the 2D image content.

The disadvantages of image content based object reconstructions are highly application dependent and the parameters and conditions of the algorithms must therefore be adjusted for each specific kind of image. But because some parameters such as lightning could be regulated and the measurements will be done on the tires with some known parameters this kind of disadvantages could be reduced.

Stereovision

The aim of the stereo based methods is to obtain 3D information about 3D objects from 2D images acquired with “ordinary” cameras. The usage of two cameras solves the problem of the ill-posed camera of the image content method. The stereo based methods are probably the most widely used set of methods for obtaining 3D information about existing objects and scenes.

The stereo based methods are all based on some form of stereoscopic vision, the same method used as a part of the human visual system. Figure 26 illustrates the stereovision setup, consisting of two cameras.

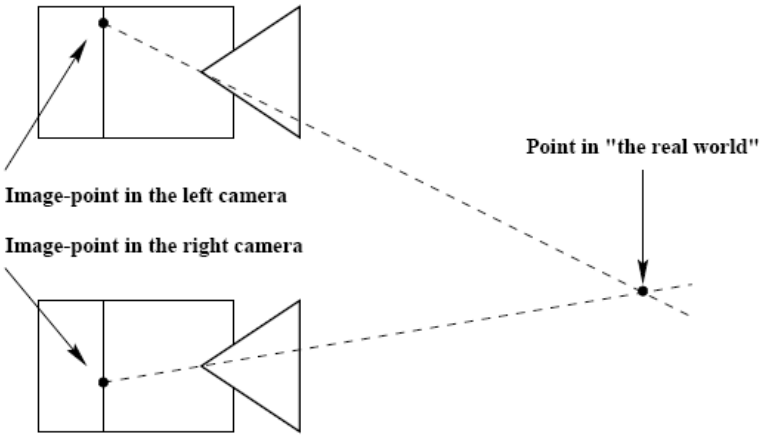

Figure 26: Stereovision setup

Apart from what might be inferred from the size, etc., of the objects in the scene, it is therefore not possible to determine the distance to the original 3D points.

The 3D point corresponding to a given 2D image point must be located on the line extending from the image point through the optical center and out into the real world. If the projection of the same 3D point can be found in two images obtained at two different positions then the two corresponding lines extending from the two image points can also be found. The intersection of these two projection lines will determine the 3D position of the original 3D point.

A prerequisite of finding the projection of the same points is one of the draw backs of the stereovision with two cameras. This can be done in numerous ways, but usually involved determining some image features. Depending on the camera setup (and the features to match) this will have a varying degree of complexity.

Feature matching will be difficult when depth measurements will be done on a dark object with changing geometry, like a tire.

Another factor against the stereovision system is that using a setup with nearly the same complexity where one camera is replaced with a laser will result in a more simple depth recovering algorithm.

Focus/defocus

The focus/defocus based methods are based on an analysis of the blurring of multiple images of an object captured with a single camera from a fixed position but with the camera focused at different (known) depths for each image.

The focus based methods are based on the way the images normally are formed by the lens in a camera. The lens of a camera refracts the light rays from 3D points through the lens, so that the rays converge and all intersect at a single point behind the lens. If the camera is focused at the distance of the 3D point then the point of intersection of the rays will be on the image plane- therefore be sharp. If the camera is not focused, the ray emerging from the 3D point will intersect in front or behind the image plane, generating a blurred image.

Theoretically these methods could be unified with the geometric triangulation principle. Fundamentally, the depth sensitivities of DFF (Depth from Focus) and DSD (Depth from Defocus) do not differ from those of stereo based systems having the same physical dimensions. However, they are more stable than stereovision (Schechner and Kiriati, 2000). But these methods do not avoid the problems of stereovision (e.g. occlusion).

Also a complexity of the construction for the focus/defocus setup is a negative aspect compared to other measurement devices.

Summarizing:

The stereovision and focus/defocus methods have a similar construction complexity as of the active sensing methods. But they don’t provide directly range data containing the 3D information as with active sensors. To investigate the possibility of using the Image content method for tire profile measurements an additional study with experiments is needed.

4.2.1 Image content

The measurement setup consists of a CMOS camera positioned on the tire. The camera parameters and their relation to the required precision are described in Appendix I. The idea of this method is using an image made with one camera to reconstruct the needed object features. By changing the camera position images with different perspective could be acquired. One possible required image and the position of the camera relative to the tire is illustrated in Figure 27.

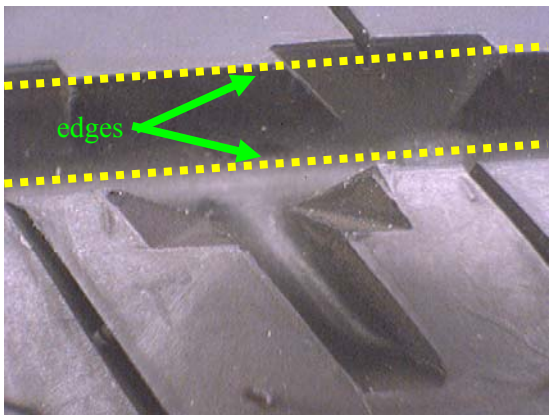

Figure 27: Image (left) and the related camera position (right)

This position of the camera (perpendicular to a longitudinal groove) is chosen because it gives the possibility for automatic search of edges for tire profile measurements (see Figure 27). The camera is placed on a construction which secures a reproducible position of the camera relative to the tire. This means that each measurement is done from the same angle and at the same distance between camera and tire. The exact knowledge of the camera position is crucial in computations of the tire profile depth (see Appendix 1). Images made with another camera position and the possible solution for profile measurements are described in Appendix II. To make the search of edges possible a proper lightning system is required. This could be achieved by placing several LED's near the camera in the measurements setup. When the edges are detected the next step is to reconstruct the metric value of the profile depth. The information which could be derived from the image is a 2D projection of the 3D real world point. To construct a reconstruction algorithm first a mathematical model of the solution is needed.

The camera model given in equation (3) expresses the projection of any 3D point on the image plane. However, it does not give a direct solution to the back-projection problem. If both radial and tangential distortion components are considered, there is no analytical solution to the inverse mapping (Heikkilä, 1997).

A nonlinear search is required or an approximation of the inverse model is needed.

The pinhole camera model is used to achieve the inverse camera model.

Suppose P' is the projection of a point P_i (see Figure 24) with known image coordinates (u_i', v_i'). To reconstruct the real location (X_i, Y_i, Z_i) of point P_i the inverse transformation consists of the inverse perspective projection, the inverse translation and the inverse rotation should be applied to the projection P'.

Metric values of the pixel coordinates can be found as follows: $\begin{bmatrix} \tilde{u}_i \\ \tilde{v}_i \end{bmatrix} = \begin{bmatrix} (u_i'-u_0)/D_u s_u \\ (v_i'-v_0)/D_v \end{bmatrix}$.

The inverse projection of a pinhole model is expressed as:

$$\frac{f}{z_i}\begin{bmatrix} x_i \\ y_i \end{bmatrix} = \begin{bmatrix} (u_i'-u_0)/D_u s_u \\ (v_i'-v_0)/D_v \end{bmatrix} \Leftrightarrow \begin{bmatrix} x_i \\ y_i \end{bmatrix} = \begin{bmatrix} z_i(u_i'-u_0)/fD_u s_u \\ z_i(v_i'-v_0)/fD_v \end{bmatrix} \quad (5)$$

With known or achieved camera parameters $(f, u_0, v_0, D_u, D_v, s_u)$ during a calibration procedure there are still two equations with three unknowns. This is the so called "ill-posed" problem which mathematically can be solved by introduction of the third equation.

Assume that the ill-posed problem is solved. The camera coordinates of the point (x_i, y_i, z_i) are calculated. With the next step the inverse rotation and translation can be performed by using the following matrix equation:

$$\begin{bmatrix} X_i \\ Y_i \\ Z_i \end{bmatrix} = M^{-1} \begin{bmatrix} x_i - x_0 \\ y_i - y_0 \\ z_i - z_0 \end{bmatrix} = M^{-1} \begin{bmatrix} z_i(u_i'-u_0)/fD_u s_u - x_0 \\ z_i(v_i'-v_0)/fD_v - y_0 \\ z_i - z_0 \end{bmatrix} \quad (6)$$

This equation gives the back-projection of a point from the image plane to real world coordinates, where M^{-1} is the inverse of a rotation matrix, known from the construction of the setup or achieved using a calibration procedure. To be able to use back-projection a solution to the ill-posed problem is needed. This can be achieved by modeling the object geometry or/and using the orthographic model (introducing some assumptions). The next section describes both reconstruction algorithms.

4.2.2 Reconstruction algorithms

As the goal of the project is recovering specified 3D information from a single view the so called "ill-posed" problem (for each point there are two equations and three unknowns) is undeniable. With other words a system consisting of one camera is always underdetermined.

For man made objects (e.g. tires), geometric constraints on the object (e.g. perpendicularity and orthogonality) can be used to solve an ill-posed problem. Also the position of the camera in the measurement system in combination with specific object geometry could add assumptions to solve the ill-position problem or to simplify the reconstruction algorithms. But in the case of free objects (with unknown geometry) this assumptions are not valid and another measurements system is needed.

4.2.2.1 Object geometry (general solution)

As was mentioned the majority of man made objects have a specific geometric form. Suppose the depth *h* of the object illustrated in Figure 28 should be measured (recovered).

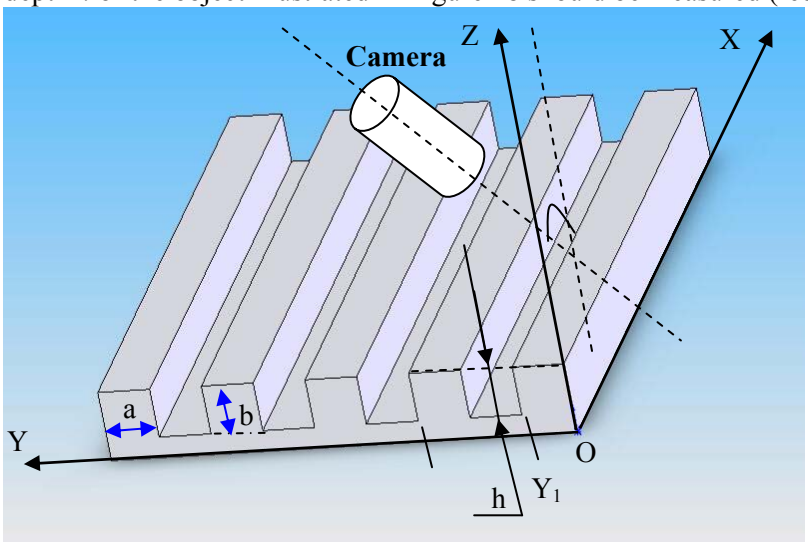

Figure 28: Right angled object

The position of the camera is as given in Figure 27 but in place of a tire an object with known geometry is used. All sides of the object are perpendicular. Measuring of the object's depth results in recovering of the real world location of the points which are belonging to the same (*XZ*) plane. Using this information equation (6) for an inverse point transformation can be rewritten as follows:

$$\begin{bmatrix} X_i \\ Y_1 \\ Z_i \end{bmatrix} = M^{-1} \begin{bmatrix} z_i(u_i'-u_0)/fD_u s_u - x_0 \\ z_i(v_i'-v_0)/fD_v - y_0 \\ z_i - z_0 \end{bmatrix} \quad (7)$$

where Y_1 is known and X_i, Z_i, z_i are three unknowns in three equations and this can be solved. When the real world locations of two points are calculated the distance between these points in 3D can be expressed as:

$$d = \sqrt{(X_2 - X_1)^2 + (Y_2 - Y_1)^2 + (Z_2 - Z_1)^2}$$

The depth *h* of an object is calculated as follows:

$$h = \sqrt{(X_2 - X_1)^2 + (Z_2 - Z_1)^2} \qquad (8)$$

Because the measurements are done on the points in the same (*XZ*) plane the factor

$(Y_2\text{-}Y_1)$ is equal to zero.

If the object's geometry is different from the one illustrated in Figure 28 equation (8) can not be used any more. The profiles of objects with different form are illustrated in Figure 29.

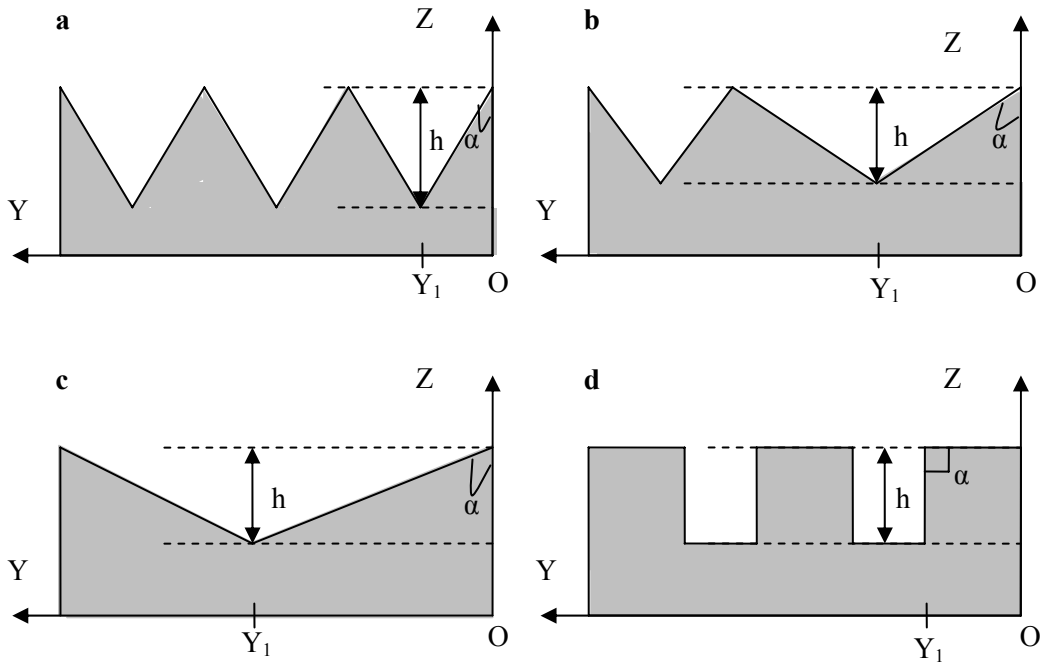

Figure 29: Different object's profiles

When the depth *h* of the objects illustrated in Figure 29 needs to be reconstructed equation (6) can be used. To solve the ill-posed problem, four different extended equations for a description of the objects geometry are required. This is the result of a change in the angle α and the shift in the position of the Y_1 point related to the camera position. The assumption, that all sides of the object are perpendicular is only valid for an object in Figure 29 d.

Summarizing:

The conclusion is that the reconstruction (measurement) of the depth *h* of the object with a known geometry is possible. But there are several draw backs to use this approach for profile depth measurements. First of all, the function in question is non-linear which means that sophisticated calculations are required to find a plausible solution. Second, the knowledge of intrinsic and extrinsic camera parameters is required and not a combination of them. This results in the need for a complex calibration procedure. Moreover, when this kind of reconstruction should be done on the objects with different geometry a database for reconstruction geometrical parameters is needed. During the life cycle of a tire the profile is burning out resulting in changes of the profile's geometry. When the geometry of the object changes frequently this can result in a frequent update requirement of the database and in the changes of the reconstruction algorithms. This is not desirable in the context of cost-efficiency.

Because of the high dependability from the object geometry another measurement method is needed.

4.2.2.2 Scaled orthographic model

A more direct approach to the reconstruction problem is based on the scaled-orthographic model.

This camera model can be used if the Z_i coordinate is almost constant in the image or when the range of Z_i values of the object points (object's depth) is small compared to the distance between the camera and the object. The maximal profile depth is nearly 20 mm. According to the orthographic model requirements the distance between the tire and the camera should be significantly longer than 20 mm. There is enough space in the wheel fender to build such construction. Only a camera with sufficient resolution is needed to meet the precision requirements of 0.1 mm.

The relation between the 3D object and its 2D image with the scaled orthographic projection is simplified as:

$$\begin{cases} u_i^{'} = s \cdot X_i \\ v_i^{'} = s \cdot Y_i, \end{cases} \tag{9}$$

with a scaling factor $s = c / Z_i$ and *c*-camera constant (Remondino and Roditakis, 2003). This scaling factor is almost constant. Therefore the whole reconstruction problem could be reduced to the problem of finding the best scale factor for a particular configuration of image points. But, the ill-posed problem is still to be solved because this model only simplifies the reconstruction problem. Only the knowledge of extrinsic and intrinsic parameters is not required. The calibration procedure is simpler and therefore more reliable than for the general solution.

To make a more realistic projection model an extension of the scaled orthographic model is needed. A reliable reconstruction result can be achieved by introduction of several scaling factors as a function of camera position related to the object.

This algorithm is tested and described in Appendix III, Scaled orthographic model.

As in the general method, additional constraints must be imposed (e.g. two object segments be orthogonal) to solve the ill-posed problem. But because the orthographic model is the base of the reconstruction algorithm this gives a possibility to introduce assumptions modeling the measured object. Although to describe the objects illustrated in Figure 29 with one model, the introduction of a huge number of approximations is needed. This will result in a high inaccuracy in the measurement results. Moreover, this method requires that no strong perspective effects are present in the image, even with the additional constrains. The strong perspective effects appear when the camera angle α (see Figure 28) is smaller than about 30°. Such position of the camera is required when the measurements on narrow grooves should be carried out. This leads also to errors in measured data. Measurements of grooves deeper than 15 mm give also unreliable results.

Summarizing:

Using the orthographic model the reconstruction problem is simplified but the structural ill-posed problem still should be solved. This method gives the possibility for some assumptions according to the object geometry. Strong perspective effects can lead to poor results. The introduction of several additional constraints can finally lead to a method with general solution, where all object's geometry should be modeled.

4.3 Active sensors

Active sensors directly provide range data containing the 3D coordinates necessary for the measurements of object depth. Consequently the measurement systems are more complex than most passive sensors, except for stereovision.

There are two different groups of active sensors. One of them is based on the measurement of the "time of flight" of a wave and another is based on triangulation. A brief description of both groups provides enough information to choose the most convenient for tire profile measurements.

Time delay

These methods are all based on some kind of measuring the "time of flight" of a wave as it travels from a transmitter to an object and back to the sensor. The "time of flight" is the time it takes from the wave leaving the transmitter until it is detected by the sensor. Based on this time measurement the distance to the object can be calculated by multiplying it by the propagation speed of the wave.

A laser range scanner is an example of a "time of flight" based setup. It works by sending a beam of laser light towards an object and measuring the difference in the phase of the emitted laser light and the returning light reflected from the surface of the object. Since both the wavelength of the laser light and the speed of light are known, the distance to the object can be calculated from the phase difference. Another method is to use a pulsed laser to send short light pulses towards the object and measure the "time of flight".

The setups based on the calculations where the speed of light is involved are used for measurements of long distances only. This is a drawback for the project. Another disadvantage is the high sensitivity to reflective characteristics of the surface.

Structured light

A setup where one of the cameras in a stereo setup is replaced by a light source emitting the structured light is called active sensing. The technique of triangulation governed by the law of sines (see Figure 30) is the basis of active sensing.

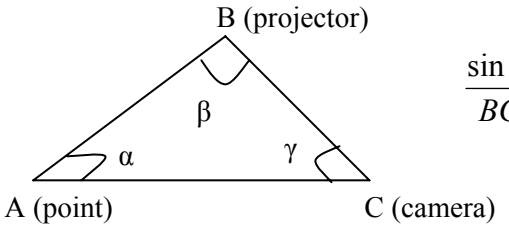

$$\frac{\sin\alpha}{BC} = \frac{\sin\beta}{AC} = \frac{\sin\gamma}{AB}$$

Figure 30: Triangulation

One of the advantages of using structured light is that the projected pattern adds features to the object, which means that inherently featureless objects also can be reconstructed. Also for objects with different geometry (see Figure 29) a universal, object independent reconstruction algorithm can be developed. The drawback of using a fixed pattern projected onto the object is that the constructed model of the object only will consists of the usually rather limited number of points created by the pattern, e.g. by the grid intersections. To avoid that problem a special kind of structured light – a laser stripe can be used.

In the most simple setup for active sensing, a spot is projected on the scene by a structured light source. The pixel address at which the point appears in an image of the scene defines the observation angle γ (see Figure 30) of the illuminated point in the scene with respect to the connecting line *BC* between camera and the projector. Using the angle β known from the setup geometry with the law of sines the distance from the camera to the illuminated point can be calculated.

More advanced techniques with intensity coding (Figure 31 a), color coding and binary coding (Figure 31 b) have been suggested as approaches to generate projection patterns with uniquely coded lines (Jørgen Bjørnstrup, 2001).

The intensity and color coding are inappropriate because of changing scene parameters. Binary coded patterns could provide a more general solution but advanced equipment is required.

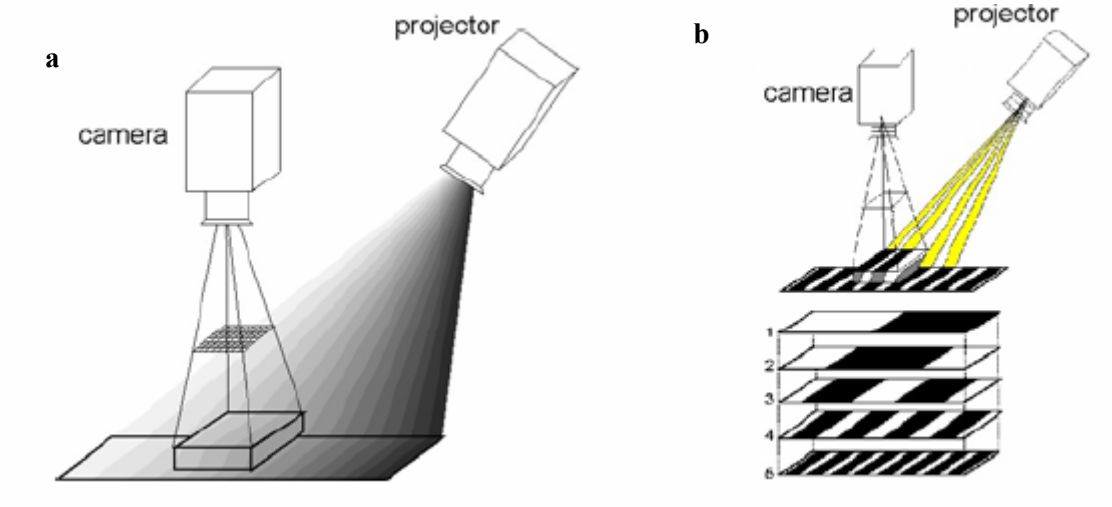

Figure 31: Intensity (a) and binary (b) coding

After comparing advantages and disadvantages of different light sources a trade-off was made. A line laser as a structured light (sheet of light) source was chosen, with in mind that the resolution of the setup can be easily improved by extending it with one or several projectors, so that a binary coded patterns could be projected. A system with mirrors is one of the solutions for creation of a virtual projector for binary coded patterns.

4.3.1 Setup description

As was mentioned, a general setup of a coded light active triangulation system consists of a camera, a pattern projector and the scene (object) under consideration (Buerkle and Fatikow, 2000). The measurement set-up is outlined in Figure 32.

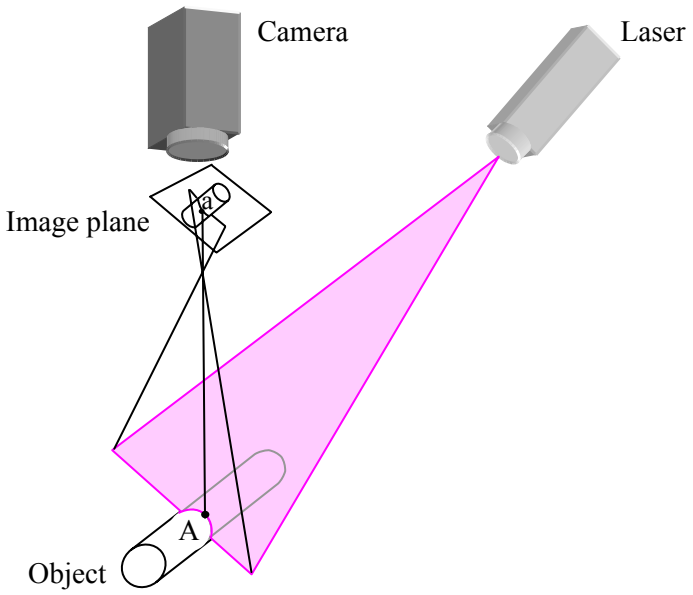

Figure 32: Setup of camera and line laser

The camera parameters are described in Appendix I. The laser has the next specifications:

- Wavelength: 625 – 670 nm
- P_{max} = 1 mW.

The distance from camera to measured object is 90 mm and the angle between the camera axis and the laser is 45°. The camera axis is perpendicular to the object surface.

The measuring principle is based on a method called “sheet of light triangulation”, a variation of a standard triangulation. A line laser generates a sheet of light that projects a curve onto the scene under the camera following the object’s profiles (see Figure 33).

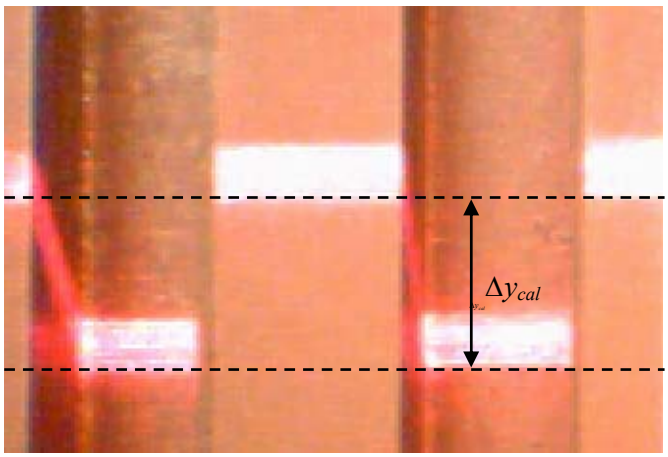

Figure 33: Image of line projected on the right angled object

The exact height of each spot on the laser line can be calculated by intersecting the corresponding camera projection ray with the sheet of light.

There are two possibilities to measure the height of an object with the described setup. The first one is a more general, geometrical approach. Therefore a calibration should be performed to obtain the camera parameters defining the pose of the camera with respect to the object coordinate system. Furthermore, the three parameters of the light plane equation $k_1 x + k_2 y + z = k_3$ must be established for the sheet of light.

The second approach is a special case making use of the object's surface. The line projected on the nearest object surface serves as a reference line. An object in the range of the laser sheet generates a displacement of the line, as illustrated in Figure 34. This offset directly corresponds to the object's height, described by the following equation:

$$\Delta h = \Delta y / \tan \varphi , \qquad (10)$$

where φ is the angle between the sheet of light and the optical axis of the camera and Δy is the displacement between reference and object lines (see Figure 34).

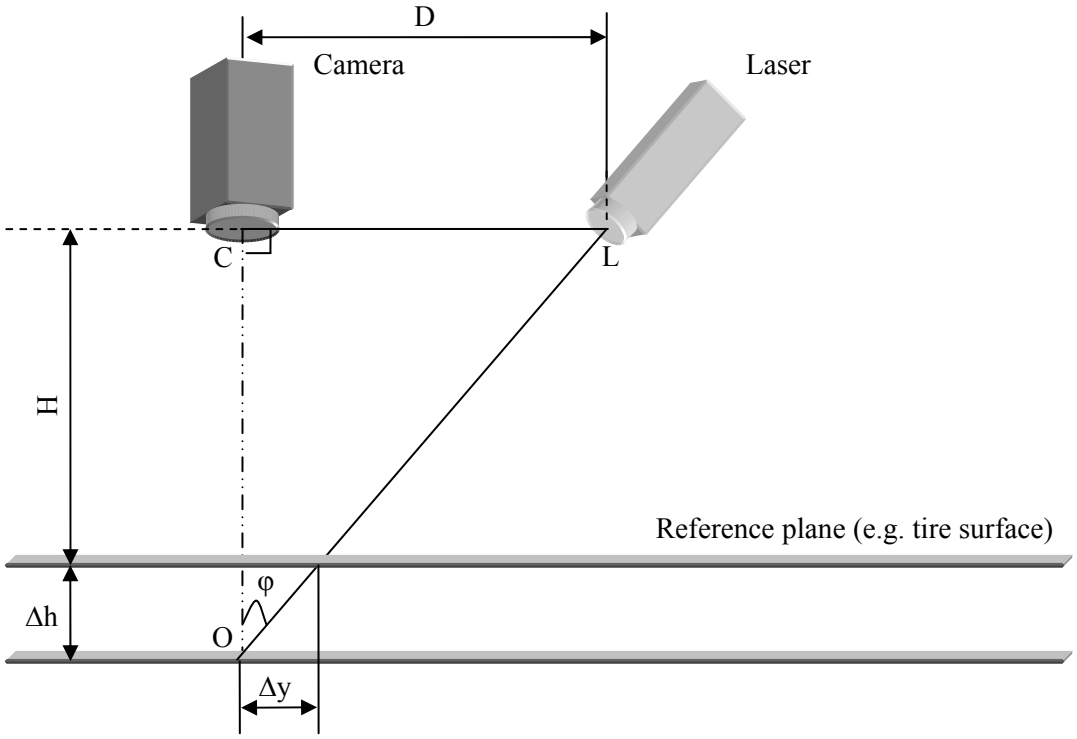

Figure 34: Parameters of setup for calculation of Δh

The accuracy that can be reached with the mentioned method depends on a several factors:

- The line segmentation accuracy (image processing)
- The CMOS/CCD camera's resolution and reliability
- The angle between the sheet of light and the camera axis

The first two factors are rather obvious and limited by the employed equipment and image processing algorithms. The third factor has a great impact on the accuracy and is interesting for fine tuning. Increasing the angle (up to 90^o) results in a higher sensitivity at the expense of a smaller effective range. An acute angle increases the effective range with loss of accuracy. The effects of various parameters on the accuracy are introduced in section 4.4 and 4.5.

4.3.2 Calibration of the triangulation system

The described line triangulation method requires two parameters in order to provide depth information:

- A calibration measure that allows a mapping between pixel coordinates and real world measurements
- The angle φ between laser sheet and optical axis of the camera.

The latter one is obtained by using a grid of dots as illustrated in Figure 35.

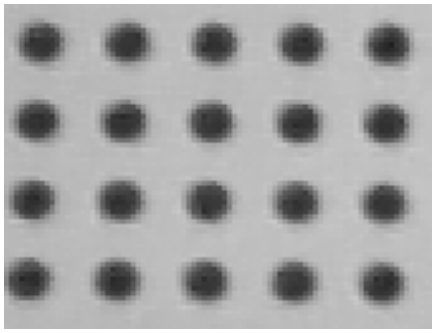

Figure 35: Grid of dots

An automated calibration procedure of Vision Assistant has been used.

To find the angle φ between laser sheet and optical axis of the camera a calibration object with a known geometry (see Figure 28) is used. The image acquired with the camera is illustrated in Figure 33. The angle is found by the following calculation:

$$\varphi = \arctan(\Delta y_{cal} / \Delta h_{cal}),$$

where Δy_{cal} is a measured metric value and $\Delta h_{cal} = b$ is known from the object geometry.

4.3.3 Results

In Figure 36 the image for the measurement of a tire profile is given. The construction of the measurements setup is shown in Figure 34.

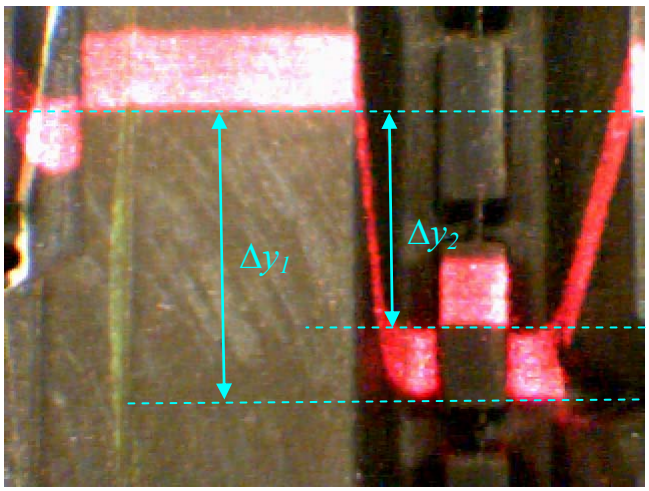

Figure 36: Tire profile measurements

The detection of the most upper and lower edges (in the image) can make an automated search of the profile depth possible. The implementation of the automatic profile measurement algorithm in Vision Assistant is given in Appendix IV. When the distance Δy_1 is measured this value should be corrected with the value of the angle φ as follows:

$$\Delta h_1 = \Delta y_1 / \tan\varphi$$

If the angle between the sheet of light and camera axis is 45° the height resolution is equal to the lateral resolution.

4.3.4 General performance tests

For this test the object illustrated in Figure 9 is used. The camera of the measurement system is positioned at 90 mm from the object's nearest surface. The angle between the sheet of light and the camera axis is nearly 45°. In Figure 37 two grooves, one 4 mm and another 2 mm wide are presented. The depth of the groove is 10 mm.

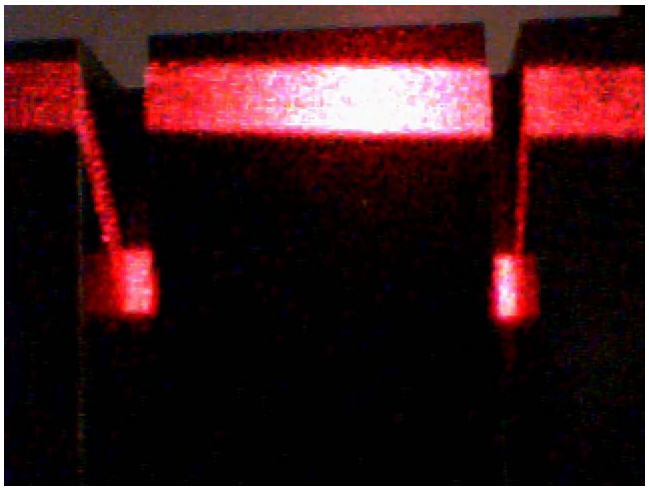

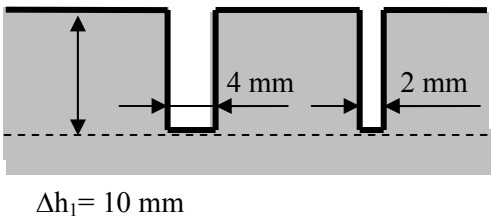

Figure 37: Grooves 4 and 2 mm

In the image both grooves can be identified. The laser sheet projected on the bottom of both grooves is visible with the camera. This gives the possibility to measure the groove's depth. Depth measurements of grooves with widths down to 2 mm are possible with the current setup.

4.3.5 Precision tests

In Figure 38 the image and the measured object (right) are given.

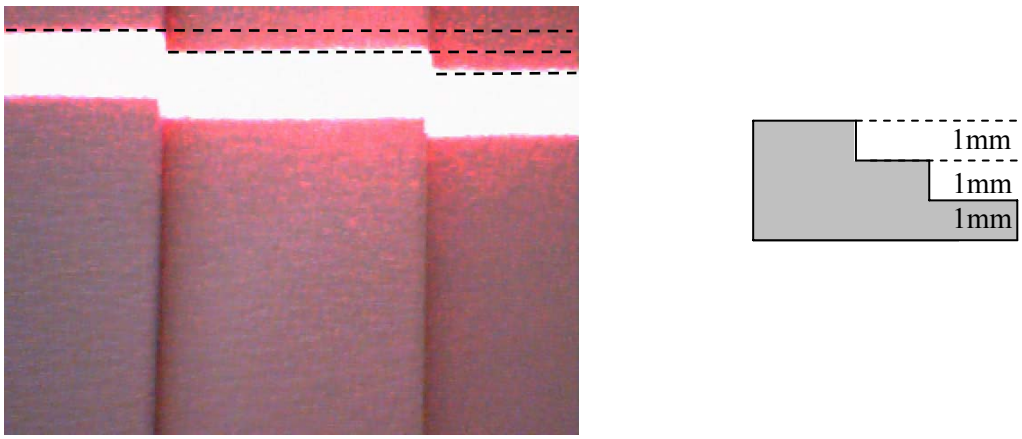

Figure 38: Three objects each 1mm high (right) and their image

It is visible from the image that the detection of a 1 mm difference in the objects height is possible. The results of several measurements state that a precision of 0.1 mm can be achieved.

4.3.6 Evaluation tests

According to the first two general performance and precision tests the active sensing method meets the measurement requirements. To control the setup performance different tires with a new and a worn-out profile is tested. Changes in the environment as lighting which could affect the measurement results are simulated as well.
The image of the worn-out tire acquired with the measurement setup is given in Figure 39.

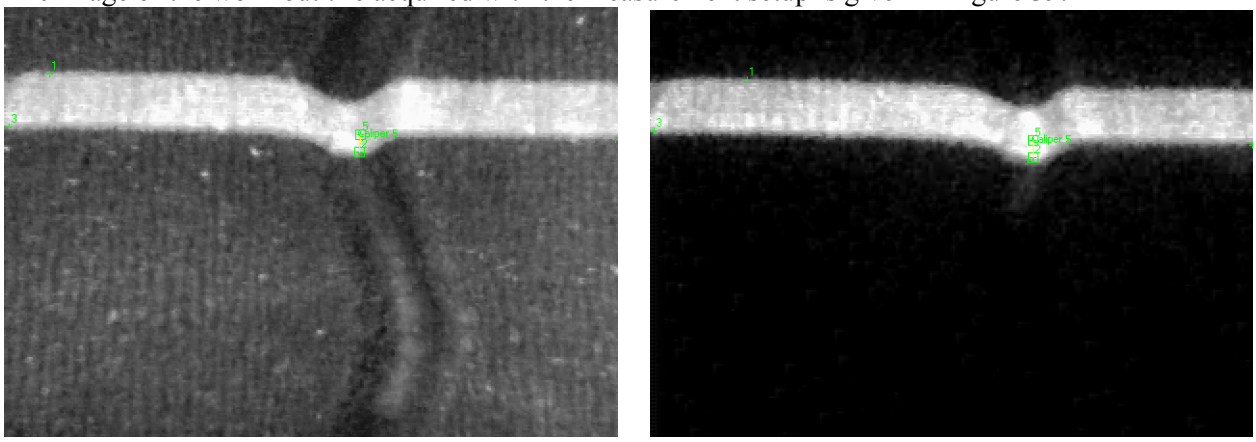

Figure 39: Worn-out tire profile 1.5 mm. Left in day light and right in darkness

The tire profile is 1.3 mm and the same value is achieved by the measurements.

Figure 40 illustrates the measurements of a new tire with a profile without a longitudinal groove. Profile depth is 18 mm. The same measurement algorithm is used for both lighted and non lighted tires. The results of the measurements are identical.

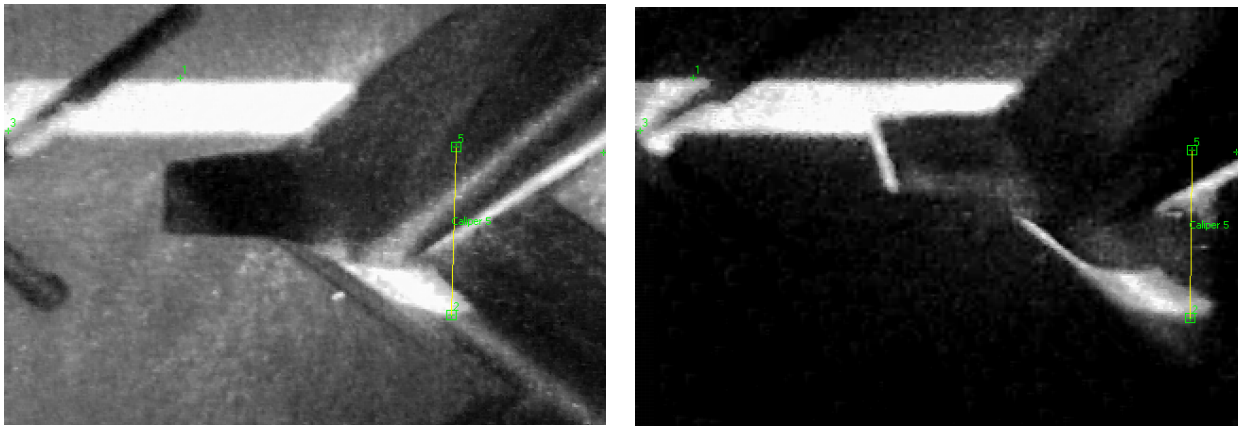

Figure 40: Tire without longitudinal groove. Left in day light and right in darkness

The sides of the groove are nearly at a right angle relative to the tire surface. Because of these factors the angle between laser and the camera axis is reduced to 30°- 35° to make it possible for the laser light to reach the deepest point of the groove. This will result in less precision, as will be shown later.

To avoid loss of precision a second laser (L2) positioned as illustrated in Figure 41 right could be applied.

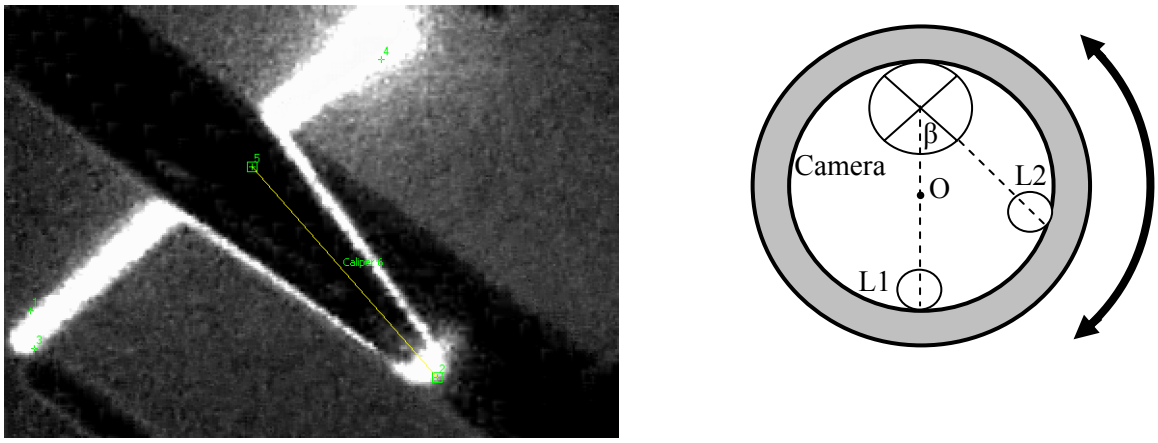

Figure 41: Light projected with a second laser at β = 45° relative to the first one

The left side of Figure 41 shows the image acquired with the camera and light projected from the second laser. The angle between the lasers is chosen as 45° because of the geometry of the tires. Most of the tires without longitudinal grooves have the grooves at nearly 45° with respect to the rotation direction of the tire (see section 2). A precise value of this angle is not needed.

A construction as shown in Figure 41 (right) could reduce the setup to one laser. L2 is the position of the laser when the construction is rotated from position L1 with 45° (centre in point O). The described construction could be used on all tire types. The position of the laser could be installed during the positioning of the measurements system on the truck. But to increase the redundancy of the system the usage of two independent lasers is preferable. The usage of mirrors to simulate the second laser can also reduce the costs of the measurements system.

4.4 Error analysis

Fluctuation in geometric parameters of the measurement system could lead to loss of measurement accuracy. The most critical fluctuations are changes in the camera and laser positions. The distance D (see Figure 42) between camera and laser is out of interest because this could be easily realized as stable and is not directly used in the calculations.

Changes in other geometric parameters can be divided in two groups:

- Internal - between camera and laser. The changes in the angle φ will be analyzed.
- External- between a measurement system (camera and laser) and the measured object. Changes in the distance H will be discussed in this case.

4.4.1 Internal

The fluctuation in the angle φ could lead to loss of accuracy. There are three situations when this angle is changed: the camera is turned, the laser is turned and when both of them are turned. All these situations could be approximated with the situation where the laser is turned. This is possible because the most important parameter for calculating changes is the angle φ.

The acceptable error (fluctuation) in the angel φ can be achieved from equation (10). Assume ε_h is an acceptable error in the profile measurements as a result of fluctuation $\Delta\varphi$ in the angle between camera and laser sheet (see Figure 42).

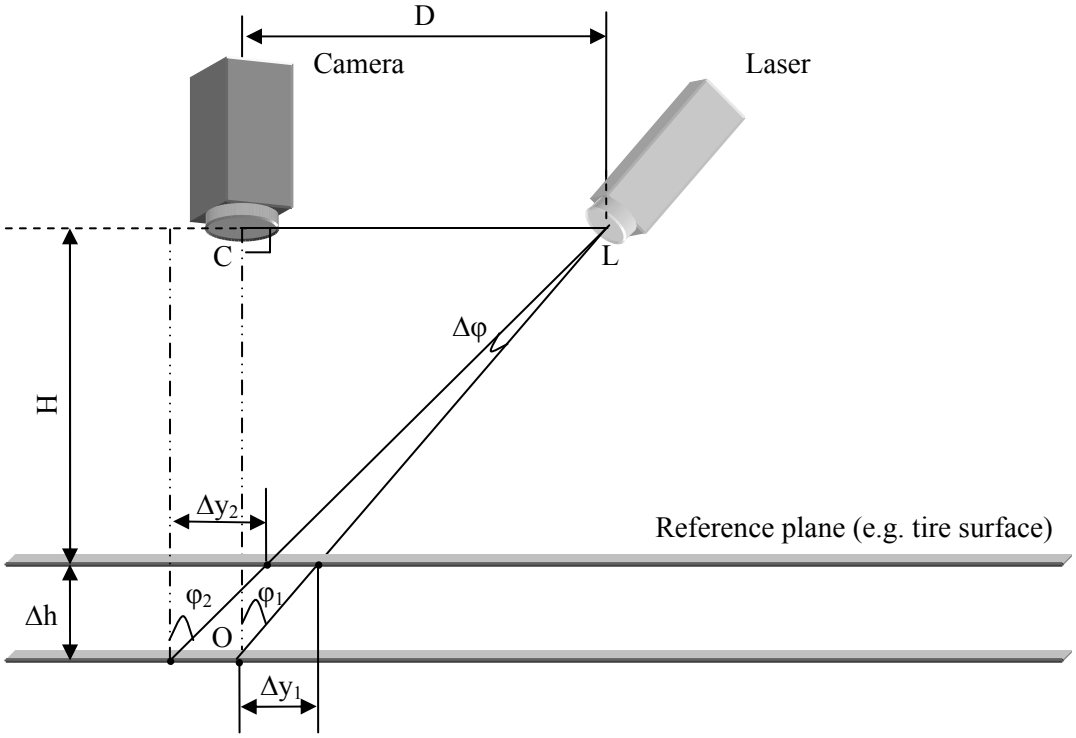

Figure 42: Angle fluctuations

The equation (10) for two cases without and with presence of an error in the angle can be written as:

$$\Delta h_1 = \Delta y_1 / \tan \varphi_1$$
$$\Delta h_2 = \Delta y_2 / \tan \varphi_2 \qquad (11)$$

With the acceptable error in profile measurements the error in the value of Δy can be recalculated as follows:

$\varepsilon_y = \varepsilon_h \cdot \tan \varphi$.

Seeing that Δh_1 and Δh_2 are equal (the same profile depth) and rewriting Δy_2 and φ_2:

$\Delta y_2 = \Delta y_1 + \varepsilon_y = \Delta y_1 + \varepsilon_h \cdot \tan \varphi_1$,

$\varphi_2 = \varphi_1 + \Delta\varphi$,

results in the equation of acceptable error in angle φ:

$$\Delta\varphi = \arctan\left(\frac{(\Delta h_1 + \varepsilon_h) \cdot \tan \varphi_1}{\Delta h_1}\right) - \varphi_1 .$$

The graphic of the acceptable angle error for different angles between laser sheet and camera axis is illustrated in Figure 43.

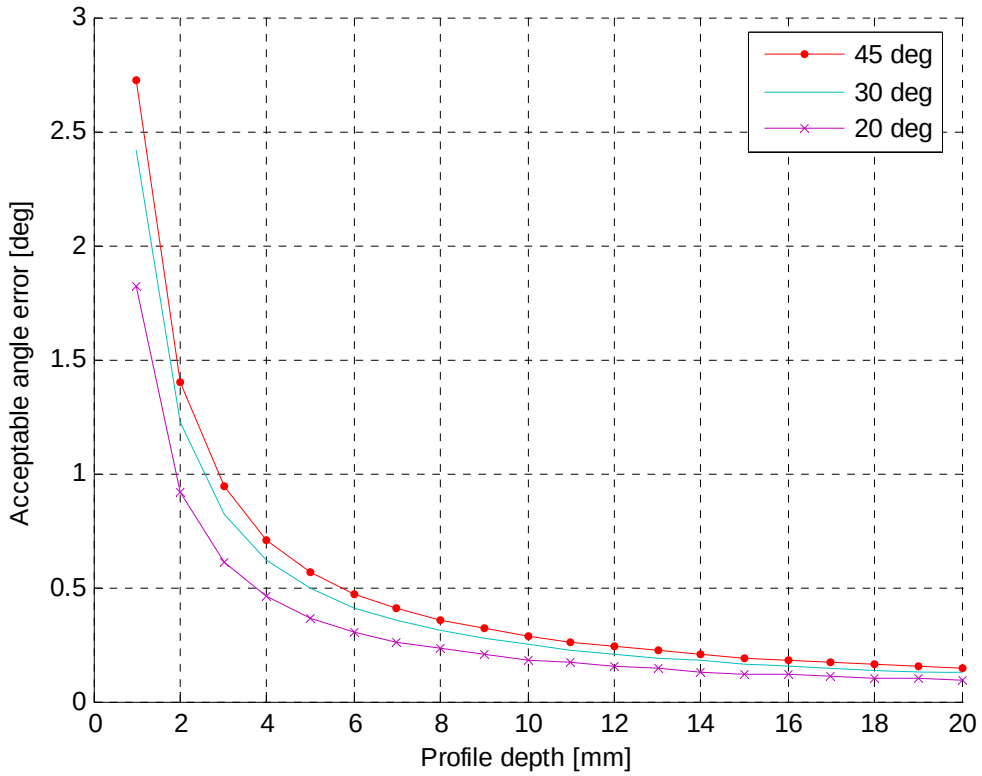

Figure 43: Acceptable angle error

For ε_h a value of 0.1 mm is used. The curve for angle φ of 60° coincides with the 30°. The graphic of 45° gives the maximal acceptable angle error. From the graphic the next conclusions follow:

- Decreasing the angle φ between laser sheet and camera the acceptable angle error decrease.
- Increase in the measured depth results in increase of the acceptable angle error.

The maximal acceptable angle error is nearly 0.2° for measurement systems with an angle of 30 - 60° between camera axis and laser sheet.

4.4.2 External

During the calibration information about the distance H between camera and the object's reference plane is achieved. This information is used in the computation of the profile depth. Changes in the distance H result in a measurement error. The changes in this distance can be divided in two groups according to their influence on the magnification:

- Changes of the distance in the measurements range [H; H+Δh] which result in the difference $\Delta M(H)$ in the magnification factors for the near and far objects.
- Fluctuations ε_H in the distance H which result in the variation $\Delta M(H, \varepsilon_H)$ of the difference of the magnification factors for near and far objects.

The magnification of the objects is described in the following equation:

$M = -d_i / d_o$,

where d_i is the image distance and d_o is the object distance.

The image distance of a particular camera is a constant and is located at: $f < d_i < 2f$. For the camera of the measurement system $d_i = 30[mm]$. The object distance is varied over an interval

[H; H+Δh]. Obviously, a long distance H between camera and the object results in less sensitivity to the magnification changes. At a certain value of H the changes of the magnification are negligible.

Using the fact that the biggest error in the magnification will be visible in the measurements of the largest objects and the required precision *R.P.*of 0.1 mm, the maximal magnification difference is:

$$\Delta M_{\max} = R.P./\Delta y = 0.1/\Delta y = 0.1/\Delta h \cdot \tan\varphi,$$

where $\Delta M_{\max} = M_H - M_{H+\Delta h}$ and Δy is the measurement value of the depth Δh.

But the high depth of field (≈10mm) and the fact that one of the lines of the displacement Δy is in focus (the magnification in the reference plane is equal to one) increases the maximal magnification difference with a factor of 8. With an angle φ= 40° the maximal magnification difference is:

$$\Delta M_{\max} = 0.05.$$

Rewriting the maximal magnification, the relation between the magnification difference and the distance H is:

$$\Delta M = -M_H + M_{H+\Delta h} = -d_i/(H+\Delta h) + d_i/H = d_i \cdot \Delta h/H \cdot (H+\Delta h)$$

Substituting $d_i = 30[mm]$ and $\Delta h = 20[mm]$ results in:

$$\Delta M(H) = 600/H \cdot (H+20).$$

The graphic in Figure 44 illustrates the relation between the magnitude differences and the distance H between the camera and the measured object.

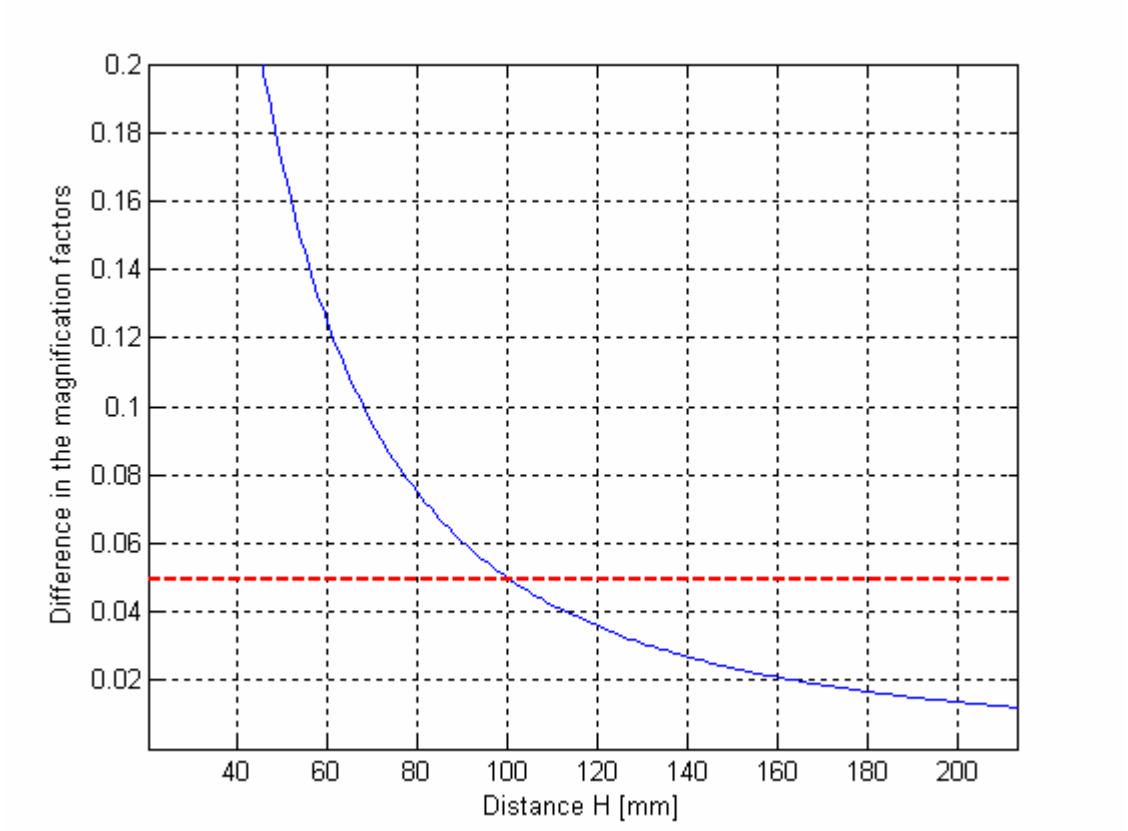

Figure 44: Difference in the magnification factors vs. distance H

The red (dashed) line indicates the maximal magnitude difference for precision of 0.1 mm. For the required precision the minimal distance between camera and the object is 100 mm. Decreasing this distance is possible but in this case a correction (to compensate for the magnification differences) in the measurement value will be needed.

To see how sensitive the measurements are to the fluctuations of the distance H, assume that the needed maximal difference in the magnification factors is achievable at all distances H between the camera and the measured object. The following equation describes the relation between

fluctuations ε_H in the distance H and the variation $\Delta M(H, \varepsilon_H)$ of the difference of the magnification factors:

$$\Delta M(H, \varepsilon_H) = d_i \cdot \left[-\frac{1}{H + \Delta h + \varepsilon_H} + \frac{1}{H + \varepsilon_H} + \frac{1}{H + \Delta h} - \frac{1}{H} \right]$$

In Figure 45 graphics for distances of 50, 70 and 90 mm between camera and the measurement objects are illustrated. The maximal variation of the difference of the magnification factor is 0.005. This value guaranties the required precision of 0.1 mm. With higher values of variation the required precision could not be achieved.

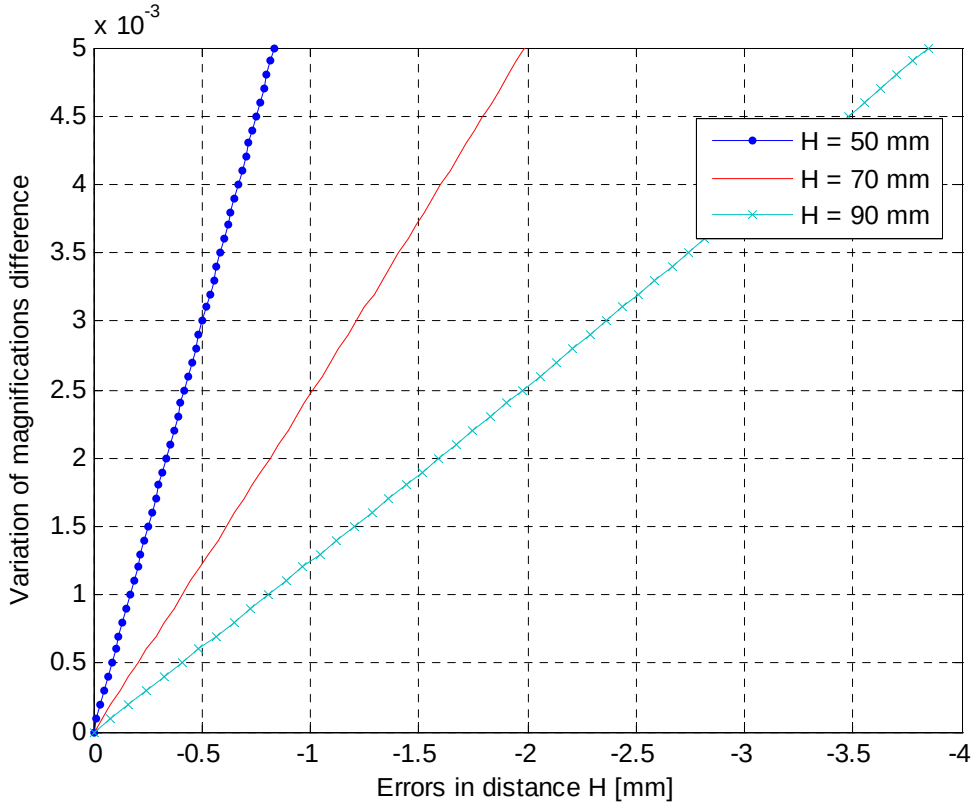

Figure 45: Variation in magnifications difference vs. fluctuation of distance H

It is visible that to achieve the same acceptable magnification error for higher values H is possible with higher fluctuation in these values. In other words the sensitivity of the measurements to the fluctuations (errors) in distance H grows when this distance decreases.

4.5 Demonstrator

For a construction of a demonstrator the geometry of the setup is changed. An additional requirement of making a geometrically small measurement setup is fulfilled. The angle β between two lasers is 45° and the distances between lasers and the camera axis have the same value. During the tests of the demonstrator setup on the objects near to maximal (20 mm) and minimal (1 mm) depths improper measurements are acquired. The analysis below describes the possible sources of inaccurate measurements. Also the solution as realized in the demonstrator is illustrated in this section.

4.5.1 Construction

The demonstrator is illustrated in Figure 46. D is the distance between the laser centre and the camera axis and H is the distance between the camera and the measured object. The distance H = 50 mm gives the needed minimal resolution and follows from the computations in Appendix I. The only possibility to minimize this distance is to use a camera with a larger angle of view.

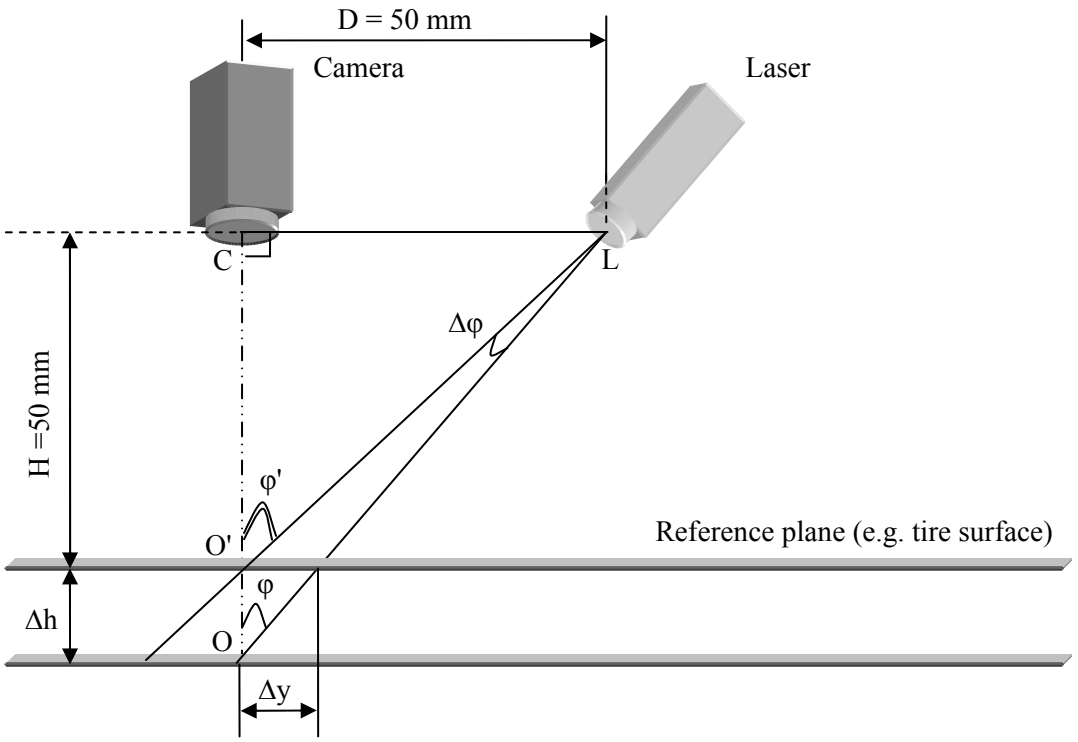

Figure 46: Demonstrator

The angle φ between camera axis and the laser sheet is defined as:
$\tan\varphi = D/(H + \Delta h)$.
Variation of D with predefined H results in changes of the angle φ. The choice of the angle is the trade off between precision, error sensitivity and the size of the setup. To prevent loss of the required resolution and for most insensitive to errors system the angle φ should be 45°. In this case the lateral resolution is equal to the height measurement resolution. For example if the angle φ is 35° the required resolution of 0.1 mm in depth measurement results in 0.07 mm ($0.1 \cdot \tan(35°)$) of lateral resolution which in its turn could be only achieved with a 1.4 times smaller value of H.
During the tests it is established that the result of the measurements with a setup with sharp angle φ gives still reliable results, so an angle of 40° between camera and laser sheet is chosen for the demonstrator. The precise value of this angle is achieved during the calibration. According to the chosen angle φ the distance between camera and laser is calculated as follows:

$D = (H + \Delta h) \cdot \tan\varphi \approx 50[mm]$,

where for Δh the maximal tire profile of 18 mm is used.
The position of the laser on the line OL will result in the same calculation and could decrease the setup size.

4.5.2 Ground of inaccuracy

From measurements with the demonstrator the following conclusions are made:

- The measured depth of the object from 20 to 11 mm is smaller than the real value
- The measured depth of the objects from 9 to 1 mm is bigger than real value
- The measurements of the object from 9 to 11 mm meat the required precision.

The error in the first two cases has a non constant character. In first case the error decreases from a maximum of 20 % of the measured value at 20 mm to zero at 10 and in the second case the error increases from zero to a maximum of 20 % of the measured value at 1 mm. Because the setup is calibrated with a 10 mm depth object the measurement of the objects between 9 and 11 mm meet the required precision.

The ground of the demonstrator inaccuracy is detected comparing two setups. The only difference between them is the position of the camera, the camera itself and the width of the sheet of laser light. Because only electronics of the camera are different and not the optical parameters the possible reaction of the measurements on changes of camera position are investigated. As the edge of the laser line is used in the measurement the depth of the sheet is the most unlikely source of the inaccuracy.

4.5.2.1 Camera

The camera in the demonstrator is placed closer to the tire than in the test setup. The distance D in the demonstrator is increased to meet the required resolution. Several factors in the geometry of the demonstrator could cause inaccuracy:

1. $H_{test} > H_{dem}$

The distance between camera and tire surface in the demonstrator is decreased.
Because the measurements are based on the angle φ the value of this angle should be precisely known. The value of the angle is achieved during the calibration with an object of a known depth (10 mm). The same value of the angle is used to translate the object with depth from 1 to 20 mm. This is possible because the changes in the angle φ for these objects are negligible. In the test setup according to the geometry the next can be written:

$H_{test} >> \Delta h$,

where Δh is the maximal profile depth.

In this case: $\tan(\Delta\varphi) = \tan(\varphi' - \varphi) = \dfrac{\tan(\varphi') - \tan(\varphi)}{1 + \tan(\varphi') \cdot \tan(\varphi)} \approx 0,$ because:

$\tan\varphi = D/(H + \Delta h) \approx D/H$

$\tan\varphi' = D/H$.

Because in the demonstrator the distance H is decreased the changes in the angle φ are not negligible anymore. A correction in this value is needed. The correction factor could be calculated from the geometry of the measurement setup or achieved from the extended calibration. Therefore, two calibration objects are needed to represent the maximal (e.g. 20 mm) and minimal (e.g. 1 mm) depths. The result of the correction can be described as follows:

$\tan\varphi = \tan(\varphi_{20} + \Delta\varphi)$,

where φ_{20} achieved from the calibration with an object with depth of 20 mm, $\Delta\varphi$ an error.

Because the angle $\Delta\varphi$ is relatively small respectively to φ and 35°<φ<45° the equation above could be rewritten as follows:

$\tan\varphi = \tan(\varphi_{20}) + \tan(\Delta\varphi)$.

Applying linear approximation for $\tan\varphi$ results in:

$$\begin{aligned}\tan\varphi &= \tan(\varphi_{20}) + \left[D/H - D/(H + \Delta h)\right] \cdot \left[(\Delta y - \Delta y_{mes})/\Delta y\right] = \\ &= \tan(\varphi_{20}) + \left[D/H - D/(H + \Delta h)\right] \cdot \left[(\Delta h \cdot \tan(\varphi_{20}) - \Delta y_{mes})/\Delta h \cdot \tan(\varphi_{20})\right],\end{aligned} \quad (12)$$

where $\tan(\varphi_{20})$ is achieved during the calibration with an object with depth of 20 mm, Δh is the maximal profile depth (20 mm), Δy is the measurement value of Δh and Δy_{mes} is the measured distance (see Figure 46).

The factor $(\Delta y - \Delta y_{mes})/\Delta y$ is a weighting factor depending on the object depth.

For the extended calibration with two objects equation (12) could be written as follows:

$$\tan\varphi = \tan(\varphi_{20}) + \left[(\tan(\varphi_1) - \tan(\varphi_{20}))/(\Delta y_{20} - \Delta y_1)\right] \cdot \left[\Delta y_{20} - \Delta y_{mes}\right], \quad (13)$$

where Δy_{20} and Δy_1 are the measured values of the objects respectively with 1 and 20 mm depth, $\tan(\varphi_1)$ and $\tan(\varphi_{20})$ are found as respectively $\Delta y_1/\Delta h_1$ and $\Delta y_{20}/\Delta h_{20}$. All this values are

achieved during the calibration. When Δy_{mes} is measured, the corrected angle φ for this particular object depth could be calculated as given in equation (13).

Also the difference in the magnification of near and far objects, as possibly the major reason of the inaccuracy, should be taken into account when the distance between the camera and the measured object decreases.

As was mentioned in section 4.4, to decreasing this distance H is possible but in this case a correction (to compensate for the magnification differences) in the measurement value will be needed.
In the test setup the distance H is 90 mm and in the demonstrator this distance is decreased to 50 mm. From Figure 44 it is visible that the distance of 90 mm results in a magnification difference of 0.06, which is near the maximal magnification difference. At distance 50 mm the value of the magnification difference is increased and is nearly 0.17. In the demonstrator the difference of 0.17 results in inaccurate measurements and should be corrected. The extended calibration with two objects gives the possibility to correct the magnification difference.

2. $H_{test}>H_{dem}$ and the camera is turned as illustrated in Figure 47.

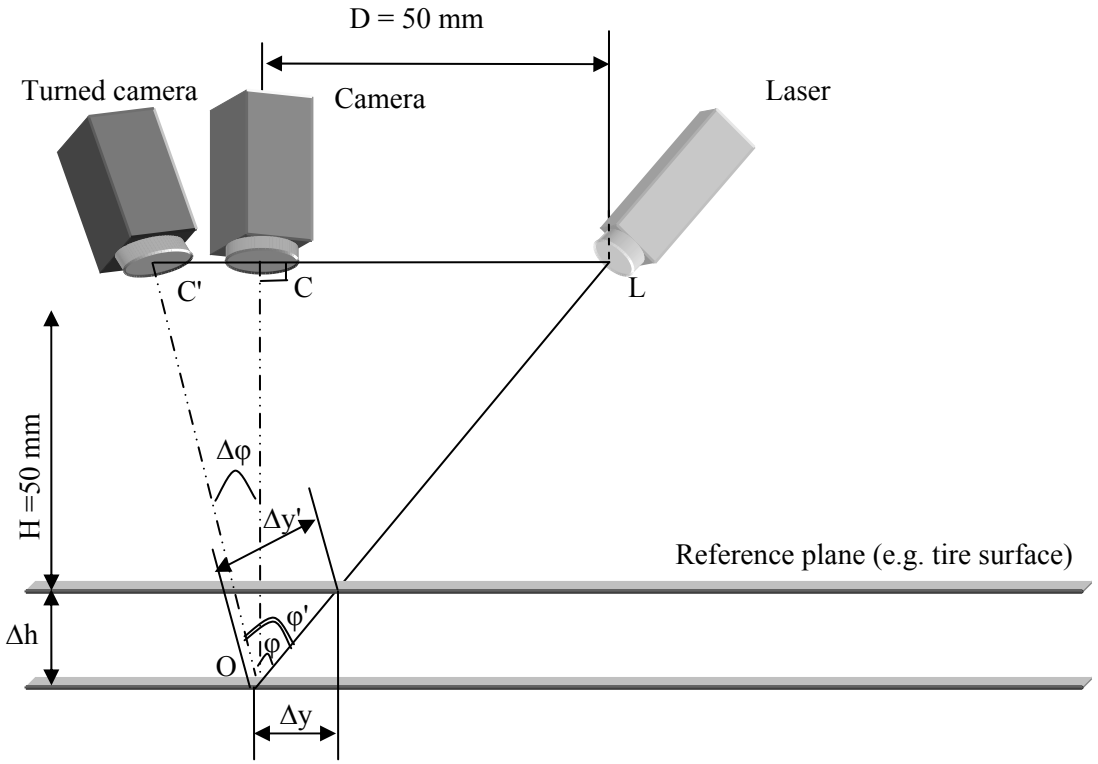

Figure 47: Camera turned

The geometry of the measurement system is changed and the angle OCL is not a right angle. The applied triangulation method will give inaccurate measurements.

During the calibration with an object of a known depth the angle between the camera axis and the laser sheet is calculated as:

$$\beta = \arctan(\Delta y'/\Delta h).$$

This is not the angle φ' which should be calculated. Furthermore when the angle φ' is found the calculation of the depth Δh of the object is complicated and involves knowledge of the geometry of the measurement system. When the angle Δφ is relatively small related to the angle φ (as illustrated in the Figure 46 and Figure 47) the approximation with correction used for the laser sheet could be applied for the correction of the camera angle. This is possible because actually both situations describe small

changes in the angle between the camera axis and the laser sheet, so the same approximation is possible.

Using a correction as defined in equations (12) and (13) for the value of the angle φ reduces inaccuracy in the depth measurements for both described cases.

The displacement of the camera from the vertical position towards the laser should be prevented. First of all this results in unnecessary loss of accuracy (decrease in angle φ). Second, for several specific grooves this could result in an erroneous measurement. For example on grooves parallel to the laser sheet the projection of the sheet on the side of the groove could be detected as a reference line. This will result in an erroneous measurement. Even though this situation is uncommon it should be avoided.

4.5.2.2 Laser

The measurements are based on the search of the laser lines projected on the object. The distance between the edges as illustrated in Figure 36 are determined. In the first setup the line width is nearly 100 pixels and in the demonstrator it is 10 pixels. The edge detection tool identifies the discontinuities in the pixel intensities of an image. The discontinuities are typically associated with abrupt changes in the pixel intensity values and in the case of the same laser they are identical. When the averaging of the intensities on the both sides of the edge is limited to 8 pixels (<10 pixel) the edge detection for both setups will give the same results.

4.5.3 Correction factor

Independently from the cause of the inaccuracy the application of a correction factor based on calibration with two objects (as discussed earlier in this section) results in reliable measurements. This is realized in the demonstrator. The reason is that the calibration is done without usage of the parameters of the camera or the geometry of the system. When evolving these parameters in the computation precise knowledge of their values is required.

4.6 Conclusions

An analysis of the most suitable method from each group of passive and active sensing systems is given, and verified by experiments. Two different approaches to find a solution for a general ill-posed problem of passive sensors are studied. This was the result of choosing the Image content as a candidate measurement method. Because of the huge number of different truck tire types there is no possibility to develop a universal measurement method. However a solution for some types is possible.

The active sensing method gives reliable measurement results. The measurement algorithm is object independent. This is the major difference from the passive sensors which results in a universal measurement method for all types of tires. A simple calibration procedure and a simple search and computation algorithm make this method robust and more suitable for a real-time performance if needed.

5 Conclusions and Recommendations

The project is finished with the realization of a demonstrator based on the most suitable method for tire profile measurements The following conclusions and recommendations can be given according to the study and the experiments carried out during this project.

5.1 Conclusions

Table 1 summarizes the results from the study and the experiments performed on the selected method of each sensors group.

Criteria \ Group	Optical	Acoustic	Active imager
Precision	-	-	+
Narrow object measurement	-	0	+
Construction	-	-	+
Environment dependence	+	+	+

+ good
0 neutral
- bad

Table 1: Comparison of the results

The comparison criteria are based on the requirements. Clearly, the best performance can be achieved with the active imaging method. The requirements are matched with the simplest construction. For both optical and acoustic measurement systems a scanning mechanism is needed, which may reduce the reliability of a practical system.

5.2 Recommendations

For better robustness of the measurements multisensing could be applied. The result of e.g. two different measurements on the same object could be compared. A large difference between two measurement results will indicate an error in the measured value of one/both sensors. When the measurement values are lying relatively near to each other, averaging values of two methods will result in more reliable measurement.

When the size of the measurement system should be minimized the usage of a wide-angle camera is suggested. The result of minimization can also be the shortening of the distance H between camera and measured object. In this case a general geometric approach is needed to achieve reliable measurement results.

Special attention should be paid when operating the camera under sharp angels in relation to the object and/or laser light. In these cases accurate camera and imaging models are required.

Appendix I – Camera parameters and precision

The precision of the distance measurements must be 0.1 mm. The setup which is used for this method includes a Logitech QuikCam camera and a PC with an image processing tool. To achieve a needed precision in distance measurements the imaging system should produce images with high enough quality. In that way an information needed from image could be extracted.

In Figure 48 the fundamental parameter of imaging system are illustrated:

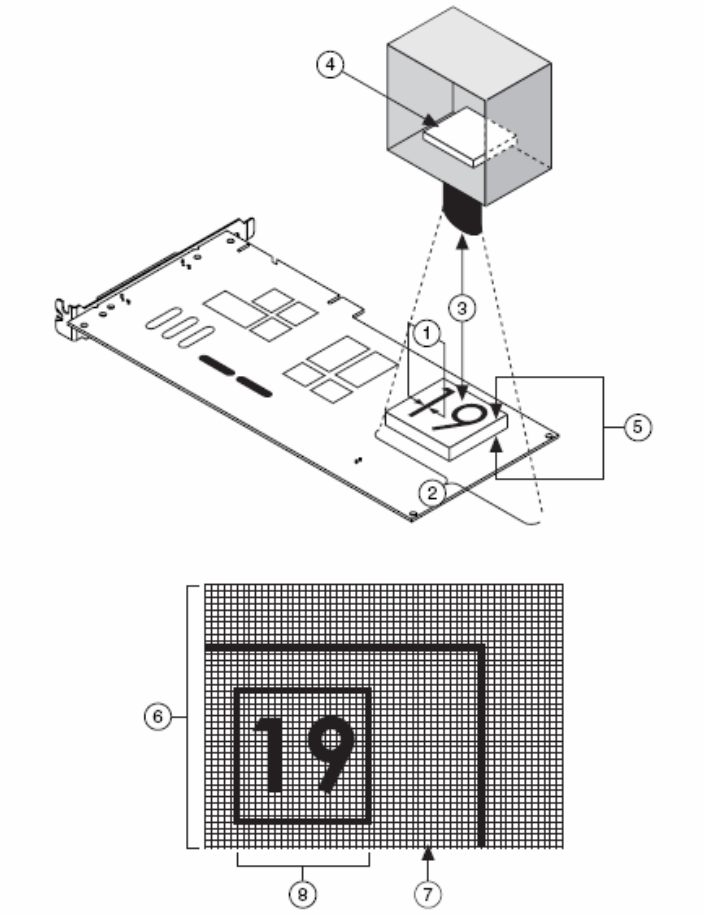

1) Resolution
2) Field of view
3) Working distance
4) Sensor size
5) Depth of field
6) Image
7) Pixel
8) Pixel Resolution

Figure 48: Parameters of an imaging system

Several factors contribute to the overall image quality: resolution, contrast, depth of field, perspective, and distortion. The primary importance has resolution.

There are two kinds of resolution to consider in an imaging system: pixel resolution and resolution. Pixel resolution refers to the minimum number of pixels needed to represent object under inspection. Minimal two pixels are needed for the representation of smallest feature. To achieve required precision two pixels must be used for representation of 0.1 mm. The image acquired from the camera has 640x480 effective pixel resolution. The maximal camera's field of view must be 32mm x 24mm for required 0.1 mm precision.

Suppose the horizontal view angle of the camera is α and vertical is β. The working distance from camera to object can be calculated using the view angel of the camera and field of view (see Figure 48). Because the image is two dimensional there are horizontal and vertical view angel, two working distances can be calculated:

d_h - when the resolution of horizontal direction is important

d_v – when the resolution of the vertical direction is important.

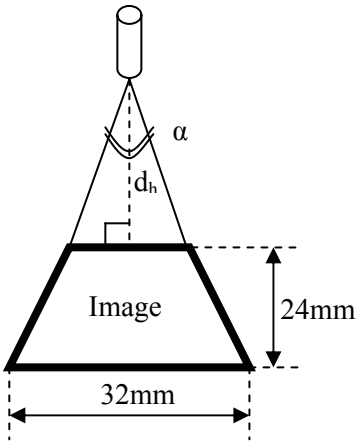

Figure 49: Calculation of maximal working distance

The maximal horizontal working distance when $\alpha = 42°$ is: $d_h = 16\text{mm}/\tan(\alpha/2) = 42$ mm.

The maximal vertical working distance when β=32° is: $d_v = 16\text{mm}/\tan(\beta/2) = 42$ mm.

Because of symmetric pixel size the horizontal and vertical resolution are the same.

Appendix II – Different camera positions

Possible solution with two different camera positions:

- Camera axis perpendicular to tire surface (see Figure 50)
- Camera axis at 45° and rotating direction of the tire is parallel with camera axis (see Figure 51).

Both measurement methods are based on the automatic search of the longitudinal groove.

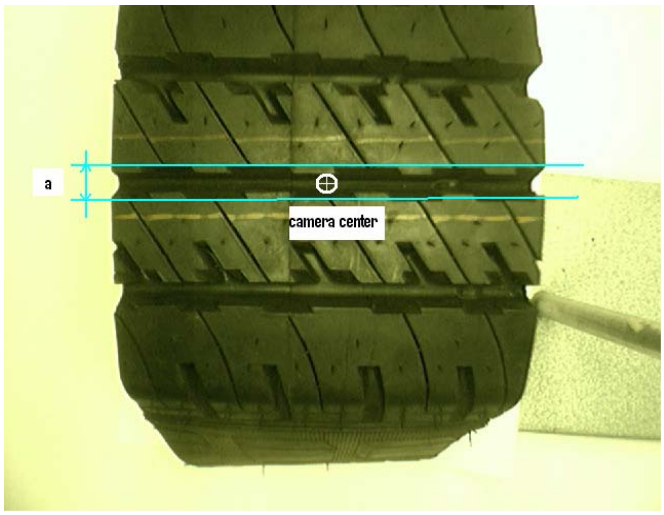

Figure 50: Camera axis perpendicular to tire surface

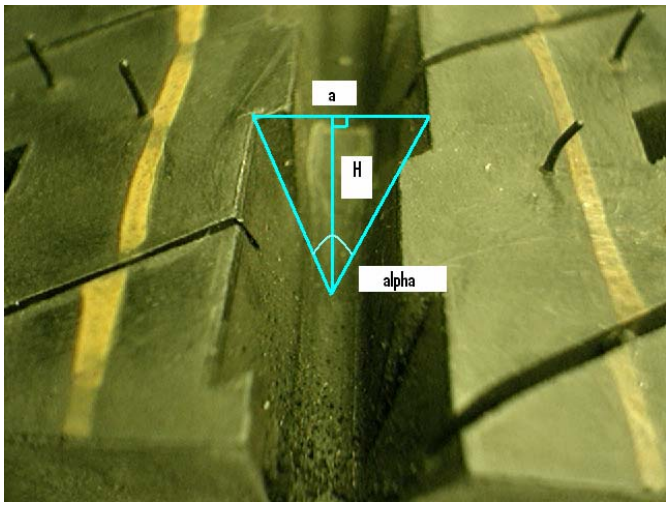

Figure 51: Camera axis at 45° to horizon

For both illustrations the following calculation can be applied.

The value of distance H is needed. Using this value the profile depth is easy calculated taking into account the treed thickness. Using triangular from the illustration next could be written:

$$H = a/2 \cdot \tan(\alpha/2).$$

The angle α is known from the tire manufacturer. Distance *a* will be measured. The precision of the calculations of H depends on the precision of the measurements of distance *a*.

Measuring at the centre of the image avoid the perceptual faults.
Advantages:

- Reliable: Distance *a* is always visible, because the measurement is based on searching for two lines in the profile.

- High independence from the changes in the vertical angles of the camera. The projection of distance *a* stays the same. The horizontal angle of the camera must be controlled by the construction. Easy to achieve by placing the camera in the middle of the tire.
- Simply calibration mechanism. The calibration grid will be placed on the tire surface, because measurement will be done on this surface. This will translate pixel value to real world values.

Disadvantages:

- Depends on the tire profile. To make the calculations of distance H possible (using angle α and distance *a*), α must have ranges from 10° to 180°. A lot of tire types have the angle α smaller than 10°. That why for a development of a universal for all tire types profile measurements method introduced technique could not be used.

Appendix III – Scaled orthographic model

The measurements setup is illustrated in Figure 28. The camera axis in all illustrations of this appendix is perpendicular to (XZ) plain. Before measuring the tire profile the camera setup is calibrated. The calibration of the measurements setup consists of two steps:

- 2D calibration

  Translation of pixel coordinates to real world coordinates. Using the grid of dots with known distances the distances in pixels will be translated to real world values.

- Depth calibration

  Computing the scaling factor as a function depended on camera position. For this step a pattern with accurately known dimensions will be used.

2D calibration

In this step a built in calibration of the vision software is used. The calibration setup is positioned as illustrated in Figure 52.

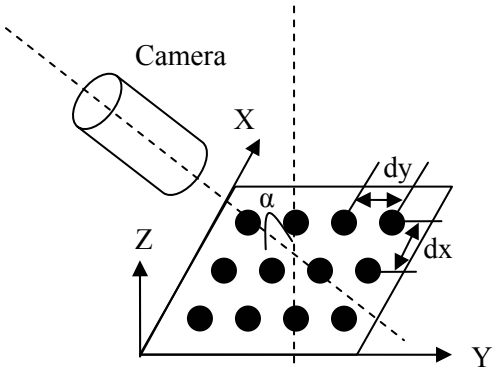

Figure 52: 2D calibration

For calibration a grid of dots in (x,y) plane is used for translation of pixels to real world values. The distances dx and dy are provided to vision software. Because the camera positioned not perpendicular (x,y) plane but at an angles α this cause perspective errors. Perspective errors appear as changes in object's magnification depending on object's distance from the lens. These errors will be corrected in software. When later a measurement on a real object will be carried out the mapping achieved during the calibration will be used to translate the pixel to metric values. Because the camera is calibrated in (XY) plane for measurements in Z direction a correction should be applied. This correction is achieved in the next calibration step.

During this step of calibration the parameters of the camera are indirectly calculated and will be used during the measurements.

Depth calibration

In Figure 28 object used for this calibration is illustrated. The position of the objects highest side is the same related to the camera as the grid of dots. Depth *b* and pitch *a* parameters of the object are known and are of the same length. Also taking into account that all object's angles are right a correction as a ration $R = a / b$ between measured and real values could be achieved.

Image acquired with the camera setup from Figure 28 is illustrated in Figure 53.

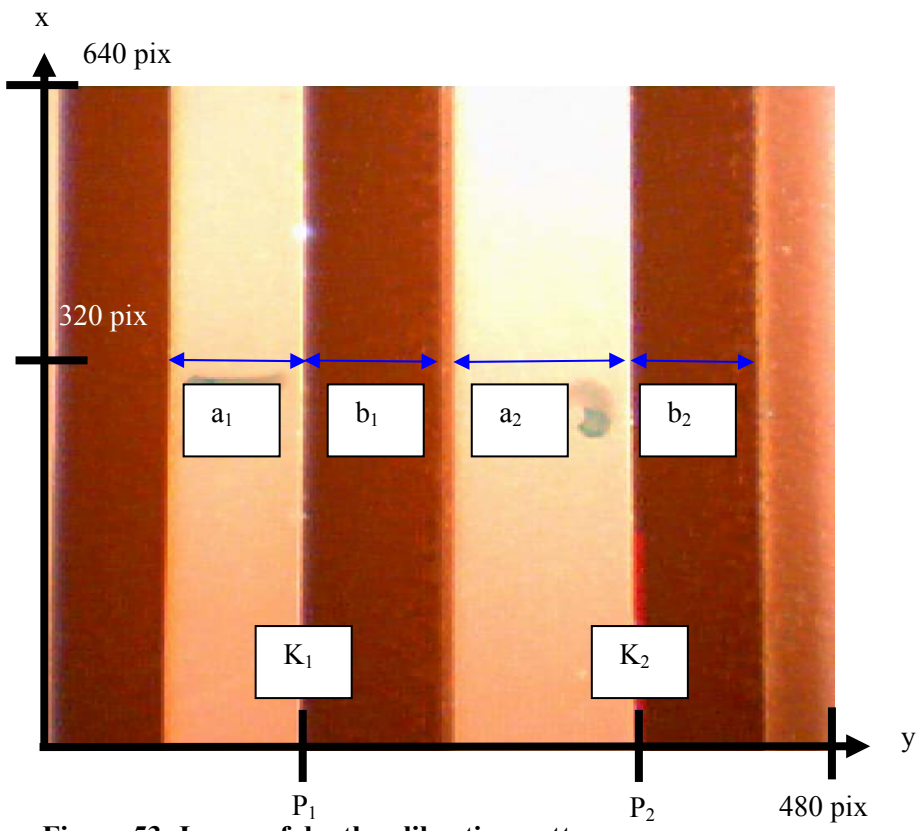

Figure 53: Image of depth calibration pattern

The distances a_1, a_2, b_1, b_2 are measured and ratios R_1, R_2 are calculated as followed:

$R_1 = a_1 / b_1$, $R_2 = a_2 / b_2$. These ratios are depended on the camera position (angles α between camera axis and the Z axis) and on the position in the image P (y coordinate) where the distances a_1, a_2, b_1, b_2 are measured. The position P in the image describes the camera translation.

The real world values of depth b and pitch a are known and in this particular example they are equal. The ratio $\Delta R/\Delta P = (R_2 - R_1)/(P_2 - P_1)$ describes a change in R per P position in the image. Using this ratio the formula for calculation of the C correction coefficient is:

$$C = ((P - P_1) \cdot \Delta R)/\Delta P + K_1 \text{ ,,} \qquad (14)$$

where P will be found during the measurements on the object and is the y coordinate of the begin point of curried measurements (see Figure 54). Using coefficient C the correction related to the camera position (angle α) and the position of the measurements in the image will be applied.

Tire profile measurements

When the camera setup is calibrated the measurements on tire can be carried out. The position of the camera during the calibration steps and the measurements on tire must be the same.
The ill-posed problem is solved assuming that the groove in the tire profile has right angles. In actuality this angles are equal to 95°. With this assumption the correction coefficient achieved during the calibration could be used for tire profile measurements.

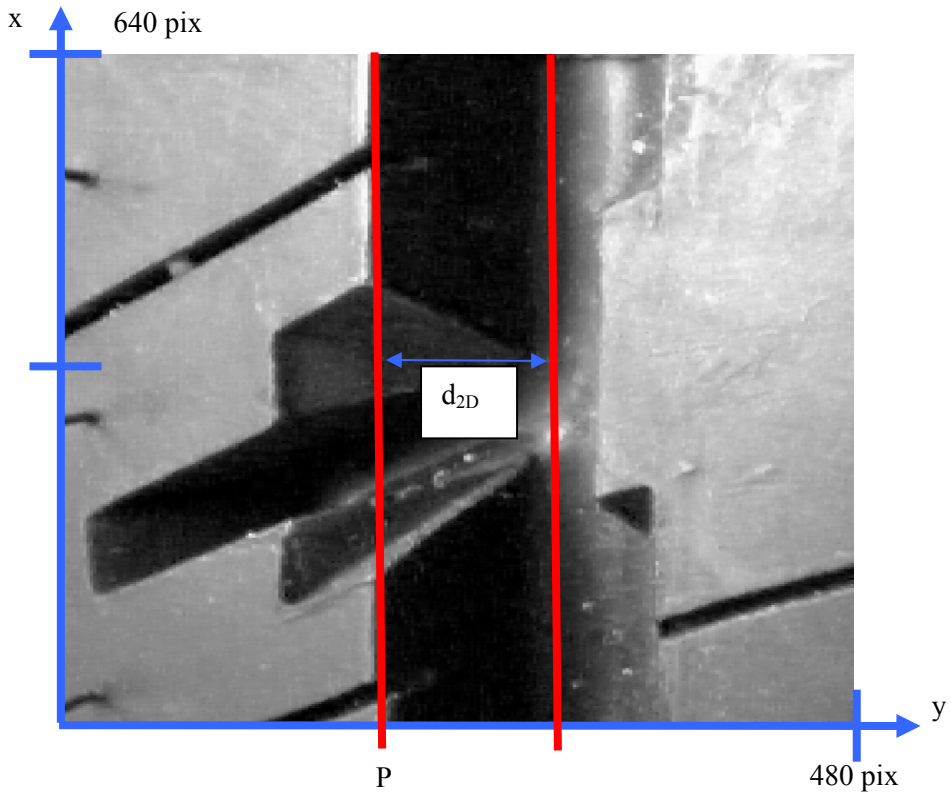

Figure 54: Tire profile measurements

The image of tire as shown in Figure 54 is acquired. To translate measured d_{2D} distance to real value the C coefficient calculated with equation (14) must be used. The real value of profile depth will be:

$d_{real} = C \cdot d_{2D}$.

Test results

The test shows reliable results with the camera angle α near 45°. With the angels sharper than 30° measurements have poor precision. The introduced algorithm can not manage strong perspective effects. For profile grooves deeper then 10 mm the measurements result are not reliable.

Both problems are the result of orthographic approach. The possible solution for this is using a camera with high resolution. This will allow placing the camera farther from the measured object what is favorable for orthographic approach.

Appendix IV – Implementation in Vision Assistant

The Figure 55 illustrates the implementation of the automatic profile measurements in the Vision Assistant.

Figure 55: Vision Assistance implementation

The algorithm consists of the following steps:

- Loading the image of the tire profile.
- The image is calibrated from an image with calibration information. The metric measurements could be applied.
- The red color is extracted to make the post processing possible, because for next steps grayscale image should be used.
- With the Clamp tool upper and lower edges are detected (see Figure 56)

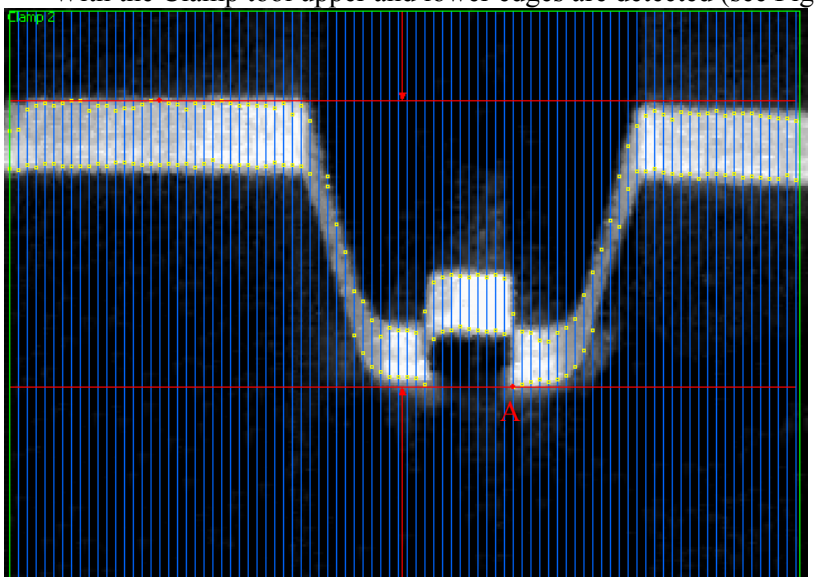

Figure 56: Clam function for edge detection

The point A from the lower edge (see Figure 56) will be used in the measurements of the tire profile.

- Straight edge as illustrated in the Figure 57 is detected.

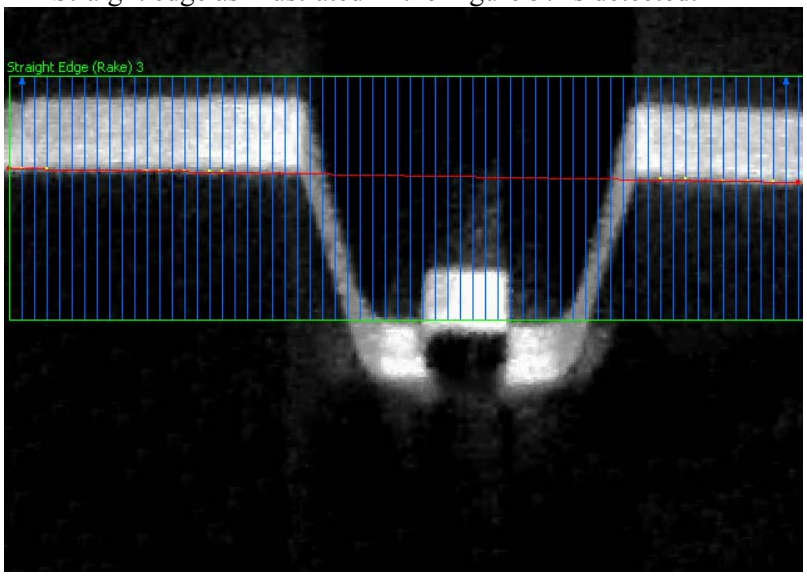

Figure 57: Straight line detection

- In the last two steps a shortest distance between the point A and the straight edge is measured.

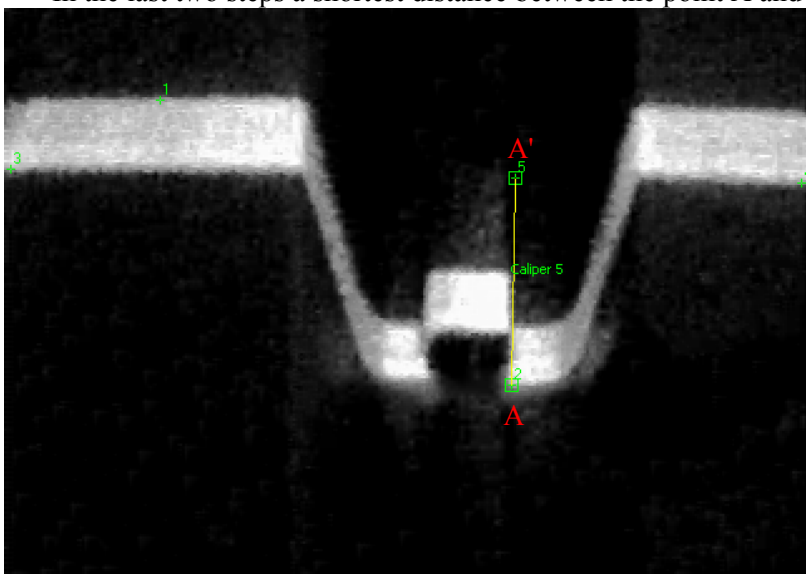

Figure 58: Shortest distance measurements

This is done measuring the distance between projection A' (on the straight line) of the point A and this point. This value is corrected with the angle between the camera axis and the laser light which is achieved during the setup calibration.

Literature

Regtien P.P.L. (2004), Measurement systems for mechatronics.

Ferdie van der Heijden (1994), Image Based Measurement Systems, *J. Wiley*

Heikkilä, Janne (1997): Accurate camera calibration and the feature based 3-D reconstruction from monocular image sequences, *Infotech Oulu and Department of Electrical Engineering, University of Oulu, Finland.*

Fabio Remondino and Andreas Roditakis (2003), Human Figure Reconstruction and Modeling from

Single Image or Monocular Video Sequence, *4th International Conference on 3D Digital Imaging and Modeling, Banff, Canada.*

Yoav Y. Schechner and Nahum Kiriati (2000), Depth from defocus vs. stereo: How different really are they?, *International Journal of Computer Vision.*

Jørgen Bjørnstrup (2001), Making 3D Models of Real World Objects, *Laboratory of Computer Vision and Media Technology, Institute of Electronic Systems, Aalborg, Denmark*.

Axel Buerkle and Sergej Fatikow (2000) Laser-based depth recovery for fine positioning of a microrobot, *Institute for Process Control and Robotics, University Karlsruhe.*

René de Ridder (2004), Optical Basic Functions and Microsystems.

Faugeras O. (2006), Three-dimensional computer vision: a geometric viewpoint.

Fabio Remondino and Sabry El-Hakim (2006), Image based 3D modeling: A Review, *The Photogrammetric Record.*

Jules Bloomenthal and Jon Rokne (1991), Homogeneous Coordinates, *Department of Computer Science, The University of Calgary*

Peter Eisert (2007), Visualisierung, Codierung und Übertragung virtueller 3D-Welten, *Institut Nachrichrichtentechnik, Heinrich-Herz-Institut*

Fox J., B. Khuri-Yakub and G. Kino (1982), High-frequency acoustic wave measurements in air, *Stanford University*

MyungKwan Shin and KyiHwan Park (2004), Study on nonlinearity of CCD sensor using optical triangulation, *Gwangju Institute of Science and Technology, Korea*

Jan Fischer, Vladimir Haasz and Tomaš Radil (2004), Simple device for small dimension measurements using CCD sensor, *Czech Technical University, Prague*

Erik van Dop (1999), Multi-sensor object recognition: The case of electronics recycling, *University of Twente.*